Manifestations of syn-eruptive fluid circulations on carbonate veins, Central Anatolian Volcanic Province

Volkan Karabacak[1], Halim Mutlu[2], and Kıymet Deniz[2]

[1]Eskişehir Osmangazi University
[2]Ankara University

November 23, 2022

Abstract

Although there are several attempts to compare the age distributions on travertines with episodes of surrounding volcanism, the correlation between the precipitation record of carbonate veins and the fractural pattern around a volcanic conduit has not yet been examined. In this study, we investigate the geochronological, geochemical and isotopic characteristics of two travertine deposits (Balkaya and Sarıhıdır) surrounded by many eruption centers in the central Anatolia with ample paleoeruption records. High-resolution carbonate precipitation records revealed by U-series dating are well correlated with the compiled dataset on Acıgöl caldera and Erciyes stratovolcano eruptions with regard to fractural positioning to the volcanic centers. Syn-eruptive carbonate precipitation is thought to occur because of sudden flux of CO-rich fluid along the extensional fracture systems aligned tangential to the related volcanic conduit and, therefore, may be an alternative technique for the reconstruction of paleoeruptions. δO and δC values of the travertine sites are within the range of meteogene fluids and δO values show a similar trend to climate proxies preserved in different depositional environments throughout the world. It is likely due to that studied carbonates were precipitated under similar fluid conditions which are represented by high rate of dilatation followed by the meteoric water influx into the extensional fracture systems.

Hosted file

`tables.docx` available at https://authorea.com/users/545208/articles/601949-manifestations-of-syn-eruptive-fluid-circulations-on-carbonate-veins-central-anatolian-volcanic-province

Manifestations of syn-eruptive fluid circulations on carbonate veins, Central Anatolian Volcanic Province

Volkan Karabacak[a*], Halim Mutlu[b], Kıymet Deniz[b]

[a] Department of Geological Engineering, Eskisehir Osmangazi University, Eskisehir, Turkey

[b] Department of Geological Engineering, Ankara University, Ankara, Turkey

*corresponding author:

Professor Volkan Karabacak, PhD
Eskişehir Osmangazi University,
Department of Geological Engineering,
26040, Eskişehir, Turkey
Fax: +90 222 2290535,
Phone: +90 222 2393750/3408,
e-mail: karabacak@ogu.edu.tr

Keywords: volcanism, carbonate vein, eruption, dating, central Anatolia

Abstract

Although there are several attempts to compare the age distributions on travertines with episodes of surrounding volcanism, the correlation between the precipitation record of carbonate veins and the fractural pattern around a volcanic conduit has not yet been examined. In this study, we investigate the geochronological, geochemical and isotopic characteristics of two travertine deposits (Balkaya and Sarıhıdır) surrounded by many eruption centers in the central Anatolia with ample paleoeruption records. High-resolution carbonate precipitation records revealed by U-series dating are well correlated with the compiled dataset on Acıgöl caldera and Erciyes stratovolcano eruptions with regard to fractural positioning to the volcanic centers. Syn-eruptive carbonate precipitation is thought to occur because of sudden flux of CO_2-rich fluid along the extensional fracture systems aligned tangential to the related volcanic conduit and, therefore, may be an alternative technique for the reconstruction of paleoeruptions. $\delta^{18}O$ and $\delta^{13}C$ values of the travertine sites are within the range of meteogene fluids and $\delta^{18}O$ values show a similar trend to climate proxies preserved in different depositional environments throughout the world. It is likely due to that studied carbonates were precipitated under similar fluid conditions which are represented by high rate of dilatation followed by the meteoric water influx into the extensional fracture systems.

1. Introduction

The internal structure of thermogenic carbonate veins is composed of alternated vertical bands that are precipitated from CO_2-rich hot waters through the fracture systems around the geothermal areas (Pentocost, 2005; Uysal et al., 2007; Brogi and Capezzuoli, 2014; Karabacak et al., 2017). The formation of these bands is closely linked to repeated precipitation episodes that require reopening of previously sealed fractures within the bedrock, favouring a temporary hydrothermal fluid circulation. Every band of the vein presents a limited time that corresponds to the period starting just after the event until sealing (Williams et al., 2017; Capezzuoli et al., 2018; Karabacak et al., 2019). Thus, since carbonate veins are highly suitable for direct dating of calcite, they provide an opportunity to understand the history of fluid circulation in a region of seismic or volcanic unrest.

Most of the previous studies devoted to carbonate veins focus on the interaction with fluid circulation and active crustal deformation (e.g. type and direction of regional stresses, dilatational rate) (e.g. Altunel and Karabacak, 2005; Uysal et al., 2007; Brogi et al., 2017). In recent works, their relations with earthquake strain cycles are also addressed (Uysal et al., 2011; Brogi and Capezzuoli, 2014; Williams et al., 2017). Moreover, it is proven that the age distributions of vertical bands in a carbonate vein supply direct dates of the nearby fluid flow circulation in the areas of seismic unrest (Karabacak et al., 2019). These features make the carbonate veins quite attractive for the active tectonic studies.

In volcanic regions, deformation is caused by shear failure, tensile failure or fluid pressurization process that produce ruptures at the tip of a magma body during strain cycles (Anderson, 1951; Rubin and Gillard, 1998; Azzarro, 1999; Glen and Ponce, 2002; Zobin, 2003). Stress in a radial-pattern spreading generates extensional fractures positioned tangential to volcanic conduits (e.g. Anderson, 1951; Macdonald, 1972; Park, 1989; Borgia et al., 2014) thus creating deep migration pathways for the fluids. During strain cycles, changes may also occur in deep aquifers (Montgomery and Manga, 2003; Wang et al., 2004) that are loaded by great elastic strain at depth (Seed and Idriss 1971), resulting in a relatively large expulsion of depressurized CO_2-rich hot waters. Therefore, subsurface hot fluids are mobilized in deeply penetrating fractures that act as conduits for hot waters and as a result, carbonates are precipitated around the volcanic eruption centers.

The previous studies asserted the temporal correlation between carbonate precipitation and volcanism with random sampling strategies on travertine deposits, carbonate veins and speleotherms (e.g. Tuccimei et al., 2006; Priewisch et al., 2014; Karabacak et al., 2017; Weinstein et al., 2020). For example, Priewisch et al. (2014) suggest that the deposition ages of voluminous travertines overlap with the episodes of basaltic volcanism in New Mexico and Arizona. Karabacak et al. (2017) compare U-series geochronology of carbonate veins with previous volcanic eruption records and achieve to resolve independent events on two different eruption centers. In the literature, however, there is a lack of studies focusing on continuous precipitation record to compare the syn-eruptive fluid circulations and carbonate vein ages. Furthermore, none of the previous studies assessed the correlations regarding the fractural pattern and volcanic conduit position.

In this study, we investigate a continuous precipitation records of carbonate veins in the Central Anatolian Volcanic Province (CAVP) and evaluate precise U-Th ages, mineralogy, and geochemical and isotopic characteristics of alternated bands. We compare our results with paleo-eruption records from major volcanic centers (Figure 1). Our correlations are discussed with regard to fractural positioning to the eruption centers to discriminate the event origin. Furthermore, oxygen isotope and rare element compositions of vein samples provided us with a great opportunity to examine temporal variations in the temperature and source of fluids that precipitated the studied travertines in the region.

2. Material and Method

Mineralogical and petrographic determinations of carbonate samples were carried out at the Geology Department (YEBIM Center) of the Ankara University. Porosity types and textural characteristics of samples were studied with Leica DMLP model polarizing microscope. Mineralogical composition of carbonates was determined with Inel Equinox 1000 X-Ray Diffractometer. Raman spectroscopy analysis on selected samples was conducted with DXR brand using laser beam of 780 nm.

Carbon and oxygen isotope analyses of carbonate samples were carried out with micromass Isoprime dual inlet isotope ratio mass spectrometer (DI-IRMS) at the Environmental Isotope Laboratory of the University of Arizona. Samples were reacted with dehydrated phosphoric acid (H_3PO_4) under vacuum at a temperature of 70^0C. The isotope ratio measurement is calibrated based on replicate measurements of international standards NBS-19 and NBS-18. The analytical precision is ±0.1‰ for $\delta^{18}O$ and ±0.08‰ for $\delta^{13}C$ (1σ).

The trace element analyses of the carbonate samples were performed at the Radiogenic Isotope Laboratory, the University of Queensland on a Thermo X-series ICP-MS with instrument conditions as described in Lawrence and Kamber (2006), after dissolving the carbonates in a 2% HNO_3 solution embed with internal standards. The raw data were corrected for the low, detectable blank, internal and external drift, and for oxides and doubly charged species. Instrument response was calibrated against two independent digests of the USGS reference W-2, and confirmed by analysis of other inter-lab references, treated as unknowns. Corrections were applied for oxides using formation rates determined from pure single element REE standards.

Carbonate samples were dated by U-series technique at the Radiogenic Isotope Laboratory at the University of Queensland using a Nu Plasma HR Multicollector Inductively Coupled Plasma Mass Spectrometer (MCICP- MS) following the analytical protocols described in Zhao et al. (2001) and Ünal-İmer et al. (2016). $^{230}Th/^{238}U$ and $^{234}U/^{238}U$ ratios were calculated using decay constants given by Cheng et al. (2000). U-series ages were estimated using the DensityPlotter 8.5 (Vermeesch, 2012).

3. Geological Setting

3.1. Central Anatolian Volcanic Province

The tectonics of the Anatolian Block is governed by interactions between three major plates; African, Arabian and Eurasian plates. Owing to this outstanding location, the Anatolian block represents an intraplate deformation resulting from the northward convergence of the Afro-Arabian plates to the Eurasian plate. As commonly expected within intraplate domains controlled by collisional margins, the central part of Anatolia has witnessed an intense Neogene-Quaternary volcanic activity associated mainly with subduction events (Innocenti et al., 1975; Aydar et al., 1994; 1995; Piper et al., 2002).

The central Anatolia is shaped by a triangular frame controlled by Quaternary faults; NW-SE-trending Tuzgölü Fault Zone (TFZ) in the west, NE-SW-trending Ecemiş Fault Zone (EFZ) in the east and the Central Kızılırmak Fault Zone (CKFZ) in the north. The TFZ and EFZ consist of Holocene faults with strike-slip component (Dirik and Göncüoğlu, 1996; Emre et al., 2011). The CKFZ present a southward arc-shape geometry through the Kızılırmak River (Toprak, 1994). It consists of Quaternary normal faults and linements of faults with strike-slip component (Dirik and Göncüoğlu, 1996; Emre et al., 2011) and constitutes the northern margin of the CAVP (Toprak, 1994). The region of triangular frame, so called the CAVP, is surrounded by a number of eruption centers such as major composite volcanoes and monogenetic cones with voluminous volcanic products (Toprak and Göncüoğlu, 1993). In this province, Quaternary eruption development has been controlled by three main eruption centers (Acıgöl caldera, Hasandag and Erciyes stratovolcanoes) within an area of 40 km radius. Hasandağ and Erciyes composite volcanoes were formed along the TFZ and EFZ (Pasquare et al., 1988; Toprak and Göncüoğlu, 1993). The Acıgöl Caldera area lies in the central part by monogenetic cones. Paleoeruption events on extrusive materials in the region were dated by a range of methods (for the last 190 ka) (Table S1).

3.2. Balkaya and Sarıhıdır travertine sites

In the current study, we focus on fracture systems and their carbonate veins in Balkaya and Sarıhıdır travertine sites around the Avanos town that is surrounded by well-known volcanic centers between the Acıgöl caldera and Erciyes stratovolcano. In the area, Kızılırmak River flows towards west by drawing a southward arc.

Figure 2 presents the geological setting of the study area that was improved from Köksal and Göncüoğlu (1997) and Koçyiğit and Doğan (2016) authors' field observations. In the study area, Mesozoic-aged metamorphites (Köksal and Göncüoğlu, 1997) comprise the basement and are overlain by the Upper Cretaceous-Lower Paleocene granitoid-syenitoid and Middle-Upper Eocene limestones (Koçyiğit and Doğan, 2016). Volcaniclastic sediments consisting of tuffaceous fluvial deposits (Upper Miocene-Pliocene) form a huge platform at the south of

Kızılırmak River and become thinner to the north (Köksal and Göncüoğlu, 1997; Koçyiğit and Doğan, 2016). The Upper Miocene-Lower Pleistocene fluvial and lacustrine deposits are represented by tectonically controlled margins and lie on the hanging walls of the normal faults (Koçyiğit and Doğan, 2016). The studied travertines are exposed as separate bodies at the Sarıhıdır and Balkaya sites in northern part of the Avanos town.

3.3. Syntectonic fluid circulation

During seismic release, deep aquifers are loaded by larger elastic strain which causes a relatively huge expulsion of depressurized CO_2-rich hot waters (Montgomery and Manga, 2003; Wang et al., 2004; Berardi et al., 2016; Karabacak et al., 2017) giving rise to carbonate precipitation within fractures that serve as conduits for CO_2-charged groundwater (Sibson, 1987; Altunel and Karabacak, 2005). Although both high flux of CO_2 and large rate of groundwater discharge are the ultimate drivers of carbonate vein precipitation in deeply-penetrating fractures, climate-driven near-surface hydrological changes may also play an important role in episodic CO_2-rich fluid circulation. Recent studies have shown that the timing of vein formation coincides preferentially with colder and drier climate regimes (Uysal et al., 2019). Such carbonate vein precipitation is, therefore, a direct record of the seismic release during glacial periods (Uysal et al., 2007; 2011; Brogi and Capezzuoli, 2014).

The internal structure of carbonate veins formed in alternated bands is closely linked to repeated crustal reactivation that requires fluid circulation (Uysal et al., 2007; Nuriel et al., 2012; Brogi and Capezzuoli, 2014; Karabacak et al., 2017; Williams et al., 2017). Karabacak et al. (2019) review the cycles of banded carbonate vein precipitation in tectonically active areas (Table 1) and suggest that 1) *coseismic period* involves the opening/reopening of fractures due to seismic release. Simultaneous fluid circulation in fracture systems and expulsion of depressurized/supersaturated hot water are resulted in rapid precipitation of carbonates on both walls of the fracture (planar). The band is formed as whitish microcrystalline calcite that is related to abundant fluid inclusions with high-CO_2 degassing, 2) during the *post-seismic period,* saturated fluids still discharge with relatively slow flow rate until the fracture is completely plugged. Because of slow degassing rates, light-transparent macrocrystalline calcites are precipitated and 3) until the next seismic event no more carbonate could be precipitated under slow-flowing conditions. This *interseismic period* forms a hiatus with the former carbonate band.

4. Results

4.1. Sampling

We investigated the structural features reported in the previous studies in the neighborhood of study area (i.e. Toprak, 1994; Köksal and Göncüoğlu, 1997; Emre et al., 2011a; 2011b; Koçyiğit and Doğan, 2016) using digital elevation data at ca. 29-m ground pixel resolutions (AsterGDEM v2) (Figures 1, 2 and S1). The key morphological lineaments were determined by satellite images (from Google Earth software) and confirmed by field observations (Figure 2). Accordingly, main lineaments controlling the northern margin of the Kızılırmak valley are found to extend in E-W direction with a southward arc-shape geometry.

There are two travertine sites (Balkaya and Sarıhıdır) formed on these lineaments in a few km distance. Balkaya travertines occur on a dilational jog between the NW-SE-trending dipslip faults with length of about 3 km (Figures 2 and S1b). They display a normal fault morphology on which the southern blocks have moved downward. Travertines with a well-protected morphology, consist of a main central fissure filled with carbonate vein (vertically banded compact travertines), and porous bedded travertines dipping away from the central fissures. Fracture analyses on carbonate veins show the presence of two dominant stress orientations spanning the range of 70° to 130° (Figure 2). They are controlled by two conjugated sets displaying a hybrid fracture feature.

The Sarıhıdır travertines are formed on a jogging area between a NE-SW-trending left-lateral oblique fault and a NE-SW-trending morphological lineament (Figures 2 and S1a). Most of the fissures in this site have been filled with carbonate material. Field observations and bi-directional rose diagrams plotted for the Sarıhıdır fissures and veins reveal two conjugate sets in a range of 40° to 120° (Figure 2).

For isotopic and geochemical analyses, using microdrilling technique we sampled 36 bands from four selected carbonate veins at Sarıhıdır (locations 1 and 2) and Balkaya (locations 3 and 4) sites (Table S2, Figures S1-4). We selected veins that are suitable for sampling across their entire width (wall to wall) or at least from wall to the fissure center. The sampling strategy is focused on relatively thick, detritus-free crystalline bands along the veins. All samples were labelled and signed onsite to indicate the first precipitation sides.

4.2. Mineralogical and petrographic analyses

Carbonate band samples were cut parallel to their deposition directions. The samples were polished and cleaned ultrasonically. Before the analysis, two sets were prepared: one of the sets was used to investigate the whole rock mineralogy and microtexture by XRD and another was for thin section petrography.

Carbonate samples from the Balkaya and Sarıhıdır locations are divided into several subgroups concerning their textural features and mineral sizes (Table S3, Figures S5-S8). The first subgroup of the Balkaya samples is represented by well-developed banded and flow textures and composed chiefly of idiomorph, coarse crystalline, needle-shaped calcite minerals accompanied by trace amount of kaolinite (Figure S5a, b). Results of confocal Raman spectroscopic (CRS) and electron probe microanalysis (EPMA) studies indicate that bands are made up of rhodochrosite (Figure S7) and cryptocrystalline quartzs comprise the porous parts of carbonates. The porosity type is burrowing. The second subgroup of Balkaya samples has granular (mosaic) texture with different sized xenomorphic calcite minerals (Figure S5c, d) represented by fenestral type porosity. The third group is comprised by both flow and granular textures with shelter porosity (Figure S5e, f). The fourth group shows fine crystalline granular texture with shelter and fenestral porosity (Figure S5g, h). Balkaya carbonates are formed within the cracks and fractures of micritic limestone, which consists of calcite with rare quartz. The existence of quartz may indicate occasional erosion and sediment transport by surface runoff to the deposition site.

Concerning texture types, the Sarıhıdır samples are divided into three subgroups. The first group has finely banded (flow) and granular textures and consists of fine to coarse crystalline calcite with rare quartz, pyroxene (augite), epidote and clay minerals (Figure S6a, b and S8). They typically have shelter type porosity. The second group of carbonates is characterized by finely crystalline granular texture and shelter type porosity (Figure S6c, d). Samples of this group are composed of calcite, quartz, feldspar (bytownite) and opaque minerals (manganese dioxide) (Figure S6c, d and S8). The third group presents very finely banded and well-developed flow textures with shelter and fenestral type porosity (Figure S6e-h). Clay minerals occur in the carbonate bands.

Idiomorph and coarsely crystalline, needle-shaped calcites indicate rapid crystallization from the fluid. Coarse crystalline calcite minerals grow toward the fluid direction whereas fine crystalline calcites point to crystallization under a stagnant flow regime (Rizzo et al., 2019). Because of heterogeneous crystallization, calcites show various crystal sizes. The flow rate of fluids forming this subgroup is quite varied. Sarıhıdır samples contain mineral fragments of volcanic or intrusive rocks exposed in the study area. The banded texture of Balkaya carbonates is much better developed than the Sarıhıdır samples and Mn-bearing bands are thicker for the former. Cataclastic texture recognized within the Sarıhıdır carbonate veins indicates that seismic event probably postdates the carbonate formation.

4.3. U-Th geochronology

Based on the results of XRD and microscopy studies, collected carbonate samples are coarsely crystalline and consist of almost 100% calcite minerals. Calcite fabrics are generally observed as long elongated and open columnar forms. The discontinuities between the bands (hiatus) are quite noticeable ensuring no contamination in adjacent generations (Figure 3). Most of the bands display two crystalline zones: 1) towards fracture wall, whitish microcrystalline calcites that are related to abundant fluid inclusions with high-CO_2 degassing, 2) towards fracture center, light-transparent macrocrystalline calcites that are related to slow degassing rates. For U-Th dating, carbonate vein bands were microdrilled from the whitish microcrystalline parts, immediate nearest location of the band to the fracture wall (Figure 3).

$^{230}Th/^{232}Th$ ratios of most samples (more pronounced for the Sarıhıdır samples) are lower than 10 showing the presence of detrital ^{232}Th in Balkaya and Sarıhıdır sites (Tables 2 and S4). The samples have very low U contents (6.6 to 37.4 ppb). This may imply that there might be a time gap between the vein formation and the commencement of carbonate crystallization, which led to clastic material to accommodate at the deposition site.

Regarding Sarıhıdır carbonates, U-Th dates of location 1 vary from 7.5 to 29 ka and those of location 2 are rather older and range from 66 to 82 ka within analytical errors. Location 3 from the Balkaya site yields U/Th ages in the range of 33 to 73 ka. Location 4 at this site gives a wide range of age data from 14.9 to 171 ka.

4.4. Rare earth element contents

Rare earth element + Y contents of studied travertine samples are shown in Table S5. Total REY of samples fall in a wide range from 176 to 23509 ppb. REY contents of Balkaya travertines (2.4 to 23.5 ppm) are significantly higher than those of Sarıhıdır travertines (0.2 to 2.1 ppm). REY patterns of both sample sets are 1 to 3 orders of magnitude lower than the PAAS (Post-Archean Australian Shale) values (Taylor and Mclennan, 1985) (Figure 4a). REY concentrations of Balkaya samples steeply descend from La to Y and continue with a nearly flat pattern across the HREEs. However, REY patterns of Sarıhıdır travertines maintain a horizontal position from La to Lu, except for a sharp positive Eu anomaly, which might be due to replacement of calcium by this element (e.g. Rankama and Sahama, 1950).

In the PAAS-normalized diagram, REY contents of Balkaya and Sarıhıdır travertines are compared to those of volcanic and granitoid rocks exposing in the region (Toksoy-Köksal et al., 2008). It is shown that host rocks with REY concentrations greater than travertines display a flat trend that slightly descends from La to Lu.

4.5. Stable isotopes

$\delta^{18}O$ and $\delta^{13}C$ values of Balkaya and Sarıhıdır samples are given in Table 2. Carbon isotope composition of Balkaya carbonates is in the range of 11.5 to 13.2‰ (VPDB) and those of Sarıhıdır carbonates varies from 8.7 to 11.0‰ (VPDB). Oxygen isotope values of Balkaya and Sarıhıdır samples are from -11.6 to -9.5‰ (VPDB) and from -16.2 to -11.6‰ (VPDB). The data indicate that carbon-oxygen isotope systematics of Balkaya samples are higher than Sarıhıdır carbonates.

5. Discussion

5.1. Origin of fossil fluid circulations

Carbon isotope compositions of Balkaya (11.5 to 13.2‰) and Sarıhıdır carbonates (8.7 to 11.0‰) yield similar ranges. These values are higher than the array suggested for the marine limestones (±3‰; Clark and Fritz, 1997) but within the range of meteogene fluids (–3 to +8‰; Pentecost, 2005). In a previous study by Karabacak et al. (2017), $\delta^{13}C$ values of Ihlara carbonates between the Hasandag volcano and Acıgöl Caldera are reported between 7.64

and 9.31‰, which are closely consistent with the values of carbonate veins from Balkaya and Sarıhıdır sites.

As shown from the $\delta^{13}C$ vs. $\delta^{18}O$ diagram (Figure 4b), the vein systems of Balkaya and Sarıhıdır sites, although nearly 10 km apart, are represented by different carbon-oxygen isotope systematics. For example, carbonate samples of locations 1 (r^2 = 0.99) and 2 (r^2 = 0.93) from the Sarıhıdır site show a very strong positive correlation. However, location 4 from the Balkaya area is characterized by a rather low correlation with r^2 = 0.61. Figure 4b also implies that heavy isotope enrichment of samples is not restricted only to carbon but also oxygen isotope. Previous studies show that travertines deposited during rapid CO_2 degassing resulting from seismic events are enriched in both ^{18}O and ^{13}C (e.g. Pentecost, 2005; Uysal et al., 2009; Yıldırım et al., in press). According to Ercan et al. (1995) and Güleç et al. (2002), mantle-derived He contributed to the thermal fluids in the central Anatolia is almost 35% of total helium inventory. Therefore, it is likely that volcanism is the major process accounting for the high volatile inventory of the fluids in this region. $\delta^{13}C$ values of fumaroles (CO_2 gas) emitting in central Anatolia (-1.9‰) fall in the range of limestones (Mutlu et al., 2018). The difference between carbon isotope values of fumaroles and travertines in the region is attributed to CO_2 degassing from hot springs, which resulted in carbon isotope fractionation. This gave rise to the participation of heavy carbon isotope (^{13}C) into carbonate phase and enrichment of light carbon isotope (^{12}C) in the gas phase. Precipitation from isotopically enriched waters explains the isotopically heavy character of the Balkaya and Sarıhıdır carbonates.

Unlike carbon isotopes, oxygen isotopes can be used to estimate the isotope composition and/or equilibrium temperature of waters that precipitated the carbonates (Friedman and

O'Neil, 1977). The temperatures of hot spring issuing in the Sarıhıdır site and a thermal water produced from a well drilled in the same area are 29^{0}C and 44^{0}C, respectively. Assuming that discharge temperatures of thermal waters in the region have not significantly changed in the studied time interval and using the oxygen isotopic fractionation between calcite and water ($\Delta^{18}O_{calcite-water}$) proposed by Kele et al. (2015), we calculated $\delta^{18}O$ values of waters that precipitated Balkaya and Sarıhıdır carbonate veins (Table S6). Oxygen isotope composition of fluids at 29^{0}C is found in the range of -16.0 to -11.2‰ (average: -13.8‰) for the Sarıhıdır samples and from -11.2 to -9.1‰ (average: -9.9‰) for the Balkaya samples. $\delta^{18}O$ values estimated at 44^{0}C are -12.9 to -8.1‰ (average: -10.3‰) and -8.1 to -5.9‰ (average: -6.7‰) for the respective fields. These values indicate a meteoric origin for the paleowaters.

Assessment of temporal variations in oxygen isotope systematics of Balkaya carbonate veins indicates a significant decrease around 133 ka BP (Figure 6 and Table 2). Nearly 2‰ decline of $\delta^{18}O$ is most probably due to meteoric water influx into the deposition site. It is driven either by a high rate of dilatation which increased the meteoric water component of fluids or by an enhanced rainfall event in the Eastern Mediterranean land and sea regions (e.g., Bar-Matthews et al., 2003).

Throughout the late Pleistocene, the Earth has experienced periods of glacial climate terminations (glacial-to-interglacial transitions) on both orbital and millennial time scales. The long term changes in orbital parameters have led to quasi-periodic fluctuations in the eccentricity, obliquity and precession of the equinoxes with frequencies at around 100, 41 and 19/23 ka BP, respectively (e.g. Milankovitch, 1941; Berger, 1978). These quasi-cycles are originated from astronomically driven changes in the latitudinal and seasonal distributions of the solar energy (Berger and Loutre, 2004). Among these cycles, those recurring every 100-ka are prominently recorded in atmospheric CO_2 from Vostok (Petit et al., 1999), benthic $\delta^{18}O$ from the ocean cores (Martinson et al., 1987; Cortijo et al., 1994), continental ice sheets in the Northern Hemisphere (Bender et al., 1994) and speleothems throughout the world (Bar-Matthews et al., 1997; 2003; Drysdale et al., 2009). These variations are widely accepted to control the commencement of late Pleistocene glacial terminations, which are found at 23, 139, 253, 345, 419, 546 and 632 ka BP (Schulz and Zeebe, 2006).

Termination II among others received intense research over the last two decades as high-resolution U-series dates became available on carbonate meterials for which radiocarbon dating method is only possible for the last 40-50 ka. Consequently, the beginning of Termination II was elaborated by a number of studies on speleothems and benthic carbonates (136 to 129 ka BP; Gallup et al., 2002; Landais et al., 2013). In these studies, $\delta^{18}O$ was reported to decrease during warmer (interglacial or interstadial) periods. An attempt is made here to compare oxygen isotope data on Balkaya carbonate veins with records of marine benthics (Lisiecki and Raymo, 2005), and speleothems of Soreq cave (Bar-Matthews et al., 2003), Antro del Corchia cave, (Drysdale et. al, 2005), Kesang cave (Cheng et al., 2012), Buraca Gloriosa cave (Denniston et al., 2018) (Figure 5). There is a striking similarity between isotope records of travertines and global benthic and cave compilations. This implies that $\delta^{18}O$ values of carbonates deposited under open air conditions are well correlated with those of marine and subterraneus carbonates and therefore they can be used as a proxy for the climate studies.

The diagram depicted in Figure 6 yields two shoulders of $\delta^{18}O$ decrease for the carbonate veins; the first is at 122.3 ka (sample G-3) and another clustering at around 133 ka (samples

E-2, F, G-1, G-2 and H-2). These negative anomalies are separated by a relatively cooler period at 130 ka represented by a 1‰ increase (sample D1). Our data indicate that the interglacial period which started at 133 ka BP proceeded only 3 ka and then demised at 130 ka BP. This was followed by a deglaciation with a duration of 8 ka (Figure 5). Interstadial reversals are common for the glacial Termination II. The lag periods between the interglacial periods are reported 1 ka to 10 ka (e.g. Schulz and Zeebe, 2006; Moseley et al., 2015).

Alternatively, high rate of dilatation is another mechanism responsible for depleted $\delta^{18}O$ values recorded in the Balkaya travertines. The $\delta^{18}O$ of meteoric waters is strongly latitude dependent and falls in the range of −2 to −20‰ (SMOW) (Craig, 1961; Kendall et al., 1995). It is reported that during major earthquakes stable isotope ratios measured in groundwater significantly changed which cannot be explained with water-rock interaction process (e.g. Claesson et al., 2004; Reddy and Nagabhushanam, 2012; Skelton et al., 2014). These changes are caused by crustal dilatation associated with stress build-up before the seismic event, which facilitated different groundwater components to mix. Although similar isotopic variations are not previously reported in areas of volcanic unrest, it is likely that crustal deformation or high rate of dilatation during the volcanic activity may increase the rate of mixing between thermogene and meteoric waters that precipitated the travertine deposits. To test this, we examine oxygen isotope compositions of mineral waters in the Gümüşkent area (nearly 20 km NW of study area). $\delta^{18}O$ values of Gümüşkent springs fall in the range of -10.5 to -9.71‰ (Afşin, 2002) which are consistent with the estimated average oxygen isotope composition of fluids (-9.92‰ at 29°C) that formed the Balkaya carbonate veins. These values are within the range proposed for meteoric waters. It is important to note that samples with high rate of dilatation have the lowest $\delta^{18}O$ values (–10,9‰ for sample G-1) (Table 2). Assuming that $\delta^{18}O$ of springs has remained unchanged in the studied time interval, there might be significant amount of cold water influx to the deposition site of Balkaya travertines. Although limited data available, among the samples witnessed high dilatation rate, G2 and H2 are characterized by notably low rare earth element compositions (Figure 4a). This might indicate rapid ascent of meteoric waters without sufficient interaction with the host rocks (Yıldırım et al., in press).

In regard to texture and crystal size, sample D1 (dated at 130 ka) from the Balkaya travertine shows quite different mineralogical features. This sample that does not contain any banding consists of calcites with different sizes (Figure S9). In this sample, needle-shaped small calcite crystals occur along the cracks (Figure S9). The remarkable heterogeneous crystallization indicates that the continuous fluid flow with high discharge rate resulted in carbonate deposition in a turbulent environment.

We conclude that although $\delta^{18}O$ values of Balkaya travertines fall in a relatively low range, they show similar trend to climate proxies preserved in different depositional environments throughout the world. If the climatic variations are neglected, this might indicate that studied carbonates were precipitated under similar fluid conditions (by means of origin and pathway) which are represented by high rate of dilatation followed by the invasion of meteoric waters. In other words, all the samples investigated are the manifestation of crustal deformation in the region.

5.2. Manifestation of paleo-eruptions on the carbonate veins

Current deformation of the Central Anatolia measured by GPS studies is not uniform (e.g., Aktuğ et al., 2013; Simao et al., 2016). In any case, however, a regional dilatation dominates despite variations in stress directions in the CAVP (Karabacak et al., 2017). Specifically, as shown by principle strain and horizontal velocity field analyses, a tension stress striking WNW-ESE is evident around Balkaya and Sarıhıdır sites (e.g., Aktuğ et al., 2013; Simao et al., 2016). Our field analyses show that both travertine sites set on the dilational jog area along the same fault zone (i.e. along the CKFZ with 10 km-distance) and all fractures in Balkaya and Sarıhıdır sites represent notable opening features (Mode I extension fractures). There are no slickenlines on their planes and no evidence for compressional tectonics. Thus, it is concluded that the fractures were formed under the tensile stress-normal trending NNE-SSW in Balkaya and NNW-SSE in Sarıhıdır. However, although carbonate veins in extensional fractures along the same fault zones indicate close-epicenter paleoearthquakes (Karabacak et al., 2019), vein precipitation periods favouring a temporary hydrothermal fluid circulation due to seismic unrest are completely different in both travertine sites. Consequently, it cannot be asserted that Sarıhıdır and Balkaya fractures are fully controlled by the regional dominant stress orientations and/or activity of CKFZ, i.e. it requires other mechanisms. One of the main reasons of Quaternary crustal deformation in the study area is the growth of magmatic crests and associated eruptions within a fairly close region (i.e. Acıgöl caldera and Erciyes stratovolcano). Therefore, it is possible to observe the manifestations of crustal deformations related to eruptive activity in the vicinity of study area.In the volcanic regions, pressure change at the tip of magma body results in shear and tensile failures or fluid pressurization (Rubin and Gillard, 1998; Azzarro, 1999; Glen and Ponce, 2002; Zobin, 2003) and the deformation produces three types of fractures around volcanoes, i.e. radial, cone sheet and ring types (Anderson, 1951). Inflation/deflation of magma chamber or volcanic spreading form σ3 in a radial pattern and generate extensional ring fractures (e.g. Anderson, 1951; Macdonald, 1972; Park, 1989; Borgia et al., 2014). This setting forms ideal deep penetrating pathways for fluid circulations during strain cycles. Thus, the extensional fracture systems aligned tangential to the volcanic conduits could present unique manifestations of syn-eruptive fluid circulations. For example, Karabacak et al. (2017) focused on two different fracture systems in the Ihlara site (central Anatolia) and indicated different fluid migration pathways for each. The dates of carbonates in each system are correlated well with the eruptive history of the Acıgöl caldera and Hasandag stratovolcano. Assessment of their data indicates that the formation of these fracture systems in the Ihlara site is controlled by various eruption centers where they are positioned tangentially. If we consider the geometric setting of the fracture systems, Balkaya and Sarıhıdır carbonate veins have positioned tangential to the Acıgöl caldera and Erciyes stratovolcano, respectively (Figure 6). Therefore, the correlation of the timing of carbonate precipitation with paleo-eruption records in CAVP may provide significant supplementary geochronological data.

Figure S10a-c displays the U-series age distribution of carbonate veins in the Balkaya and Sarıhıdır travertine sites. The age data indicate that the vein precipitations clustered in 3 major periods in last 190 ka (i.e. 5-35, 60-100, 120-170 ka BP) (Figure S10c). Accordingly, the crustal deformation intensified during 2 different periods at about 9, 82 ka BP in Sarıhıdır (Figure S10a) and during at least 7 different periods at about 15, 22, 73, 94-100, 119, 133, 145-150, 164 ka BP in Balkaya (Figure S10b). Carbonate vein from Location 4 in Balkaya also presents a detailed continuous precipitation record for the region (Figure S11a). Figure 6a displays the U-series ages with respect to distance from the vein center to the wall. If we order the coeval bands, the graph revolves to U-series age vs. the band widths (Figure S11b) and displays that the vein has 8 rapid dilatation periods at 15, 22, 67-73, 94-100, 119, 133, 145-155, and 164-171 ka BP coherent to picks of relative probability graph (Figure S10b).

Figure S10d displays the paleo-eruption dating records in CAVP for the last 190 ka compiled from the previous studies (Table S1). Results show that the eruptions took place across the region episodically in 3 major periods (i.e. 5-40, 75-115, 145-190 ka BP) are compatible with carbonate precipitations around Sarıhıdır and Balkaya (Figure S10c). Accordingly, each eruptive period in the CAVP lasted approximately 35-45 ka and is followed by an episode of volcanic unrest of around 30 ka. Comparison of the carbonate precipitation periods (i.e. intensified crustal deformation periods) with the eruption records in the surrounding area yields that there is a great affinity between the Sarıdır results and Erciyes eruptions and between the Balkaya results and Acıgöl eruptions. For example, Holocene eruption on Erciyes Stratovolcano of 8.8±0.6 ka BP (Sarıkaya et al., 2006; 2017) was recorded at Sarıhıdır carbonate veins (sample 04; 8.8±3.8 ka BP). Similarly, an eruption dated at 22.3±1.1 ka BP in the Acıgöl Caldera region (Karnıyarık cone, 24 km distant from Balkaya) (Schmitt vd., 2011) was almost perfectly recorded in the Balkaya site (sample B; 22.4±2.1 ka BP). Table 3 summarizes the results of U-Th ages of the carbonate veins respect to the timing of volcanic eruption events in the surrounding region.

6. Conclusions

In the volcanic regions, while pressure change of magma chamber generates extensional ring fractures forming ideal deep penetrating pathways for fluid circulations, the extensional fracture systems positioned tangentially to eruption centers could present manifestations of fluid circulations during volcanic strain cycles. In the suitable areas, thus, high flux of CO_2-rich fluid discharge precipitates syn-eruptive carbonate veins in the fractures. Here we propose a model, carbonate veins of the extensional fracture systems positioned tangentially to a volcanic conduit provide a substantial late Quaternary paleo-eruption record for that center (Figure 6).

$\delta^{18}O$ and $\delta^{13}C$ values of travertine sites of CAVP are within the range of meteogene fluids. The significant decrease in oxygen isotope values of Balkaya carbonate veins is likely due to meteoric water influx into the deposition site. It is driven either by a high rate of dilatation that increased the meteoric water component of fluids or by an enhanced rainfall event triggered by a change in the climate regime.

Acknowledgements

This research is funded by the Scientific and Technological Research Council of Turkey (TUBITAK) (under grant # 118Y069). Datasets for this research are included in this paper and its supplementary information files (the references can be found in the paper).

References

Afşin, M. (2002). Hydrogeochemistry of CO2-rich Çorak, Karakaya and Gümüşkent mineral waters in Nevşehir, Earth Sciences, 26,1-14.

Aktuğ, B., Parmaksız, E., Kurt, M., Lenk, O., Kılıçoğlu, A., Gürdal, M.A., Özdemir, S. (2013). Deformation of Central Anatolia: GPS implications, Journal of Geodynamics, 67, 78–96.

Altunel, E., Karabacak, V. (2005). Determination of horizontal extension from fissure-ridge travertines: a case study in the Denizli Basin, southwestern Turkey, Geodinamica Acta, 18/3-4 (2005) 333-342.

Anderson, E.M. (1951). The dynamics of faulting and dyke formation with applications to Britain, Oliver and Boyd, Edinburgh and London.

Aydar, E., Gourgaud, A., Deniel, C., Lyberis, N., Gundogdu, N. (1995). Le volcanisme quaternaire d'Anatolie centrale (Turquie) : Association de magmatisme calco-alcalin et alcalin en domaine de convergence, Canadian J. of Earth Science, 32, 7, 1058-1069.

Aydar, E., Gundogdu, N., Bayhan, H., Gourgaud, A. (1994). Volcano-structural and petrological investigation of the Cappadocian Quaternary volcanism, TUBITAK Yerbilimleri Dergisi, 3, 25-42, In Turkish with English abstract.

Azzaro, R. (1999). Earthquake surface faulting at Mount Etna volcano (Sicily) and implications for active tectonics, Journal of Geodynamics, 28, 193-213.

Bar-Matthews M., Ayalon A., Kaufman A. (1997). Late Quaternary paleoclimate in the eastern Mediterranean region from stable isotope analysis of speleothems at Soreq Cave, Israel. Quat. Res. 47, 155– 168.

Bar-Matthews, M., Ayalon, A, Matthews, M., Gilmour, M., Hawkesworth, C. (2003). Sea-land oxygen isotopic relationships from planktonic foraminifera and speleothems in the Eastern Mediterranean region and their implication for paleorainfall during interglacial intervals. Geochem. Cosmochim. Acta 67 (17), 3181-3199.

Bar-Matthews, M., Ayalon, A., Sass, E., Halicz, L. (1994). Water behaviour in karstic system- Soreq Cave, Beit-Shemesh, summary of three years study. Israel Geol. Surv. Rep. # GSI/6/94.

Bender, M., Sowers, T., Labeyrie, L.D. (1994). The Dole effect and its variation during the last 130,000 years as measured in the Vostok core. Glob. Biogeochem. Cycles 8, 363–376.

Berardi, G., Vignaroli, G., Billi, A., Rossetti, F., Soligo, M., Kele, S., Baykara, M.O., Bernasconi, S.M., Castorina, F., Tecce, F., Shenet, C.C. (2016). Growth of a Pleistocene giant carbonate vein and nearby thermogene travertine deposits at Semproniano, southern Tuscany, Italy: Estimate of CO2 leakage, Tectonophysics, http://dx.doi.org/10.1016/j.tecto.2016.04.014

Berger, A. (1978). Long-term variations of daily insolation and quaternary climatic changes J. Atmospheric Sci., 35, 2362-2367.

Berger, A., Loutre, M.F. (2004). Astronomical theory of climate change. Journal De Physique, IV, 121, 1–35.

Bigazzi, G., Yegingil, Z., Ercan, T., Oddone, M., Ozdogan, M. (1993). Fission track dating obsidians in central and northern Anatolia, Bull. Volc., 55, 588-595.

Borgia, A., Mazzoldi, A., Brunori, C.A., Allocca, C., Delcroix, C., Micheli, L., Vercellino, A., Grieco, G. (2014). Volcanic spreading forcing and feedback in geothermal resorvoir development, Amiata Volcano, Italia. J. Volc. Geoth. Res. 284, 16-31

Brogi, A., Capezzuoli, E. (2014). Earthquake impact on fissure-ridge type travertine deposition, Geological Magazine, 151, 1135-1143.

Brogi, A., Capezzuoli, E., Kele, S., Baykara, M.O., Shen, C.C. (2017). Key travertine tectofacies for neotectonics and palaeoseismicity reconstruction: effects of hydrothermal overpressured fluid injection, Journal of the Geological Society, 174(4), 679.

Capezzuoli, E., Ruggier, G., Rimondi, V., Brogi, A., Liotta, D., Alçiçek, M.C., Alçiçek, H., Bülbül, A., Gandin, A., Meccheri, M., Shen, C-C., Baykara, M.O. (2018). Calcite veining and feeding conduits in a hydrothermal system: Insights from a natural section across the Pleistocene Gölemezli travertine depositional system (western Anatolia, Turkey), Sedimentary Geology, 364, 180-203.

Cheng et al. (2012). The climatic cyclicity in semiarid-arid central Asia over the past 500,000 years. Geophysical Research Letters, 39, L01705.

Cheng, H., Edwards, R., Hoff, J., Gallup, C., Richards, D., Asmerom, Y. (2000). The half-lives of uranium-234 and thorium-230, Chem. Geol., 169, 17–33.

Claesson, L., Skelton, A., Graham, C., Dietl, C., Mörth, M., Torssander, P., Kockum, I. (2004). Hydrogeochemical changes before and after major earthquake, Geology, 32, 641-644.

Clark, I., Fritz, P. (1997). Environmental isotopes in hydrogeology. Lewis Publishers, New York, 328 s.

Cortijo, E., Duplessy, J.C., Labeyrie, L., Leclaire, H., Duprat, J., van Weering, T.C.E. (1994). Eemian cooling in the Norwegian sea and North Atlantic ocean preceding continental Ice-sheet growth. Nature 372, 446–449.

Craig, H. (1961). Isotopic variations in meteoric waters. Science 133, 1702–1703.

Denniston, R. F., Houts, A. N., Asmerom, Y., Wanamaker Jr., A. D., Haws, J. A., Polyak, V. J., Thatcher, D. L., Altan-Ochir, S., Borowske, A. C., Breitenbach, S. F. M., Ummenhofer, C. C., Regala, F. T., Benedetti, M. M., Bicho. N. F. (2018). A stalagmite test of North Atlantic SST and Iberian hydroclimate linkages over the last two glacial cycles. Climate of the Past, 14, 12, 1893-1913.

Dirik, K., Göncüoğlu, M.C. (1996). Neotectonic characteristics of the Central Anatolia, International Geology Review, 38, 807-817.

Doğan, U. (2011). Climate-controlled river terrace formation in the Kızılırmak Valley, Cappadocia section, Turkey: inferred from Ar–Ar dating of Quaternary basalts and terraces stratigraphy, Geomorphology 126: 66–81.

Doğan-Külahçı, G.D. (2015). Chronological, magmatological and geochemical study of post-collisional basaltic volcanism in Central Anatolia and its spatio-temporal evolution. Earth Sciences. Université Blaise Pascal - Clermont-Ferrand II.

Drysdale, R.N., Zanchetta, G., Hellstrom, J.C., Fallick, A.E., Zhao, J.X. (2005). Stalagmite evidence for the onset of the Last Interglacial in southern Europe at 129 ± 1 ka. Geophysical Research Letters, Vol. 32, L24708, doi:10.1029/2005GL024658.

Drysdale, R.N., Hellstrom, J., Zanchetta, G., Fallick, A E., Sánchez Goñi, M.F., Couchoud, I., McDonald, J., Maas, R., Lohmann, G., Isola, I. (2009). Evidence for obliquity forcing of glacial Termination II, Science, 325, 1527–1531.

Emre, Ö., Duman, T.Y., Özalp, S., Elmacı, H., Olgun, Ş. (2011a). 1:250000 Scale Active Fault Map Series of Turkey, Aksaray (NJ 36-7) Quadrangle. Serial Number: 26”, General Directorate of Mineral Research and Exploration, Ankara-Turkey.

Emre, Ö., Duman, T.Y., Özalp, S., Elmacı, H., Olgun, Ş. (2011b). 1:250000 Scale Active Fault Map Series of Turkey, Kayseri (NJ 36-8) Quadrangle. Serial Number: 32, General Directorate of Mineral Research and Exploration, Ankara-Turkey.

Ercan, T., Matsuda, J.I., Nagao, K., Kita, I. (1995). Noble gas isotopic compositions in gas and water samples from Anatolia. In: Erler, A., Ercan, T., Bingöl, E., Orcen, S., Geology of the Black Sea Region: Proc. Int. Symp. on the Geology of the Black Sea Region, Ankara, Turkey. General Directorate of Mineral Research and Exploration and the Chambers of Geological Engineers of Turkey, Ankara, pp. 197– 206.

Friedman, I., O'Neil, J.R. (1977). Compilation of Stable Isotope Fractionation Factors of 649 Geochemical Interest. USGS Numbered Series (report), 440- KK, 11 p.

Gallup, C.D., Cheng, H., Taylor, F.W., Edwards, R.L. (2002). Direct determination of the timing of sea level change during Termination II, Science, 295, 310–313.

Glen, J.M.G., Ponce, D.A. (2002). Large-scale fractures related to inception of the Yellowstone hotspot, Geology, 30, 7, 647–650.

Güleç, N., Hilton, D.R., Mutlu, H. (2002). Helium isotope variations in Turkey: relationship to tectonics, volcanism and recent seismic activities. Chemical Geology 187, 129–142.

Innocenti, F., Mazzuoli, G., Pasquare, F., Radicati Di Brozolo, F., Villari, L. (1975). The Neogene calcalkaline volcanism of Central Anatolia: geochronological data on Kayseri–Nigde area, Geol. Mag., 112 (4), 349-360.

Karabacak, V., Uysal, I.T., Mutlu, H., Ünal-İmer, E., Dirik, R.K., Feng, Y-X., Akiska, S., Aydoğdu, I., Zhao, J-X. (2019). Are U-Th dates correlated with historical records of earthquakes? Constraints from co-seismic carbonate veins within the North Anatolian Fault Zone, Tectonics, 38, 7, 2431-2448.

Karabacak, V., Uysal, I.T., Ünal-İmer, E., Mutlu, H., Zhao, J. (2017). U-Th age evidence from carbonate veins for episodic crustal deformation of Central Anatolian Volcanic Province, Quaternary Science Reviews, 177, 158-172.

Kele, S., Breitenbach, S.F.M., Capezzuoli, E., Meckler, A.N., Ziegler, M., Millan, I.M., Kluge, T., Deák, J., Hanselmann, K., John, C.M., Yan, H., Liu, Z., Bernasconi, S.M. (2015). Temperature dependence of oxygen and clumped isotope fractionation in carbonates: a study of travertines and tufas in the 6–95°C temperature range. Geochimica et Cosmochimica Acta, 168, 172–192.

Kendall, C., Sklash, M.G., Bullen, T.D. (1995). Isotope tracers of water and solute sources in catchments. In: Trudgill ST (ed) Solute modeling in catchment systems. Wiley, New York, pp 261–303.

Koçyiğit, A., Doğan, U. 2016. Strike-slip neotectonic regime and related structures in the Cappadocia region: a case study in the Salanda basin, Central Anatolia, Turkey, Turkish Journal of Earth Sciences, 25, 393-417.

Köksal S. and Göncüoglu M. C. (2008). Nd Isotopic Characteristics of Some S-, I- and A-type Granitoids from Central Anatolia, Turkish J. Earth Sci., 17, 111–127.

Kuzucuoğlu, C., Pastre, J-F., Black, S., Ercan, T., Fontugne, M., Guillou, H., Hatte, C., Karabıyıkoğlu, M., Orth, P., Turkecan, A. (1998). Identification and dating of tephra layers from Quaternary sedimentary sequences of Inner Anatolia, Turkey, Journal of Volcanology and Geothermal Research, 85, 153-172.

Landais, A., Dreyfus, G.B., Capron, E., Jouzel, J., Masson-Delmotte, V., Roche, D.M., Prié, F., Caillon, N., Chappellaz, J., Leuenberger, M., Lourantou, A., Parrenin, F., Raynaud, D., Teste, G. (2013). Two-phase change in CO2, Antarctic temperature and global climate during Termination II. Nature Geoscience, 6(12), 1062-1065.

Lawrence, M.G., Kamber, B.S. (2006). The behaviour of the rare earth elements during estuarine mixing-revisited, Mar Chem. 100,147-161.

Lisiecki, L.E., Raymo, M.E. (2005). A Pliocene-Pleistocene stack of 57 globally distributed benthic $\delta^{18}O$ records. Paleoceanography, Vol. 20, PA1003, doi:10.1029/2004PA001071.

Macdonald, G.A. (1972). Volcanoes, Prentice-Hall, New Jersey

Martinson, D.G., Pisias, N.G., Hays, J.D., Imbrie, J., Moore, T.C., Shackleton, N.J. (1987). Age dating and the orbital theory of the ice ages: Development of a high-resolution 0 to 300,000-year chronostratigraphy, Quat. Res., 27(1), 1–29.

Milankovitch, M. (1941). Kanon der Erdbestrahlungen und seine Anwendung auf das Eiszeiten Problem, Roy Serbian Acad. Spec. Pub., vol. 133.

Montgomery, D.R., Manga, M. (2003). Stream flow and water well responses to earthquakes, Science, 300, 2047-2049.

Moseley, G.E., Spötl, C., Cheng, H., Boch, R., Min, A., Edwards, E. (2015). Termination-II interstadial/stadial climate change recorded in two stalagmites from the north European Alps. Quat. Sci. Rev. 127, 229–239.

Mutlu, H., Atıcı, G., Çınar Durgut, N., Hilton, D.R., Akar, M., Çobankaya, M., 2018, Variations in gas isotope compositions of thermal fluids in central Anatolia, Turkey, EGU General Assembly Conference Abstracts 20, 539.

Notsu, K., Fujitani, T., Ui, T., Matsuda, J., Ercan, T. (1995). Geochemical features of collision-related volcanic rocks in central and eastern Anatolia, Turkey, Journal of Volcanology and Geothermal Research, 64 (1995), 171-192.

Nuriel, P., Rosenbaum, G., Zhao, J.-X., Feng, Y., Golding, S.D., Villemant, B., Weinberger, R. (2012). U-Th dating of striated fault planes, Geology, 40, 7, 647-650.

Park, R.G., 1989. Foundations of structural geology, 2. edition, Blackie, Glasgow and London.

Pasquare, G., Poli, S., Vezzoli, I., Zanchi, A. (1988). Continental arc volcanism and tectonic setting in Central Anatolia, Turkey, Tectonophysics, 146, 217-230.

Pentecost, A. (2005). Travertine. Springer Verlag, Berlin Heidelberg, 446 p.

Petit, J.R., J. Jouzel, D. Raynaud, N.I. Barkov, J. Barnola, I. Basile, M. Bender, et al. (1999). Climate and atmospheric history of the past 420,000 years from the Vostok ice core, Antarctica. Nature, 399(6735), 429–436.

Piper, J.D.A., Gürsoy, H., Tatar, O. (2002). Palaeomagnetism and Magnetic Properties of the Cappadocian Ignimbrite Succession, Central Turkey and Neogene Tectonics of the Anatolian Collage, J. of Volcanology and Geothermal Research, 117 (3-4), 237-262.

Priewisch, A., Crossey, L.J., Karlstrom, K.E, Polyak, V.J., Asmerom, Y., Nereson, A., Ricketts, J.W. (2014). U-series geochronology of large-volume Quaternary travertine deposits of the southeastern Colorado Plateau: Evaluating episodicity and tectonic and paleohydrologic controls, Geosphere, 10, 2, 401–423

Rankama, K., Sahama, Th.G. (1950). Geochemistry. University of Chicago Press, Chicago, 912 p.

Reddy, D.V., Nagabhushanam, P. (2012). Chemical and isotopic seismic precursory signatures in deep groundwater: Cause and effect, Applied Geochemistry, 27, 2348-2355.

Rizzo, A.L., Uysal, I.T., Mutlu, H., Ünal-İmer, E., Dirik, K., Yüce, G., Caracausi, A., Italiano, F., Misseri, M., Temel, A., Bayari, S., Özyurt, N., Zhao, J-X, Deniz, K. (2019). Geochemistry of fluid inclusions in travertines from western and northern Turkey: inferences on the role of active faults in fluids circulation, Geochemistry, Geophysics, Geosystems, v. 20, issue 11, 5473-5498.

Roberts, N., Reed, J.M., Leng, M.J., Kuzucuoğlu, C., Fontugne, M., Bertaux, J., Woldring, H., Bottema, S., Black, S., Hunt, E., Karabıyıkoğlu, M. (2001). The tempo of Holocene change in the Eastern Mediterranean region: new high-resolution crater-lake sediment data from central Turkey, The Holocene, 11. 6, 721-736.

Rubin, A.M., Gillard, D. (1998). Dike-induced earthquakes: Theoretical considerations, J. Geophys. Res., 103, 10017-10030, doi:10.1029/ 97JB03514.

Sarıkaya, M.A., Çiner, A., Şen, E., Ersoy, O., Zreda, M. (2017). “Dating young lavaflows wıth cosmogenıc 36Cl: an example from the late pleistocene–early holocene Erciyes monogenetic lava domes in Central Turkey”, EGU General Assembly.

Sarıkaya, M.A., Zreda, M., Desilets,D., Çiner, A., Şen, E. (2006). “Correcting for nucleogenic 36Cl in cosmogenic 36Cl dating of volcanic rocks from the Erciyes Volcano, Central Turkey”, AGU Fall Meeting Abstracts.

Schmitt, A.K., Danis, M., Evans, N.J., Siebel, W., Kiemele, E., Aydin, F., Harvey, J.C. (2011). Acigöl rhyolite field, Central Anatolia (part 1): high-resolution dating of eruption episodes and zircon growth rates, Contrib. Mineral Petrol., 162, 1215–1231.

Schulz, K.G., Zeebe, R.E. (2006). Pleistocene glacial terminations triggered by synchronous changes in Southern and Northern Hemisphere insolation: e insolation canon hypothesis. Earth and Planetary Science Letters, 249, 326-336.

Seed, H.B., Idriss, I.M. (1971).Simplified procedure for evaluating soil liquefaction potential, J. Soil Mech. Found. Div., ASCE 97, 1249-1273.

Sibson, R.H. (1987). Earthquake rupturing as a mineralizing agent in hydrothermal systems, Geology, 15, 701-704.

Simao, N.M., Nalbant, S.S., Sunbul, F., Mutlu, A.K. (2016). Central and eastern Anatolian crustal deformation rate and velocity fields derived from GPS and earthquake data, Earth and Planetary Science Letters, 433, 89–98.

Skelton, A., Andrén, M., Kristmannsdóttir, H., Stockmann, G., Mörth, C., Sveinbjörnsdóttir, Á., et al. (2014). Changes in groundwater chemistry before two consecutive earthquakes in Iceland. Nature Geoscience, 7, 752–756.

Taylor, R.S., McLennan, S.M. (1985). The Continental crust: its composition and evolution. Blackwell. Oxford, p. 312.

Toksoy-Köksal, F., Köksal, S., Göncüoğlu, M.C., Romer, R.L. (2008). An Approach to the Central Anatolian (Avanos) Late Mesozoic Magmatism: Petrology of Cogenetic Granitic and Volcanic Rocks. 61st Geological Congress of Turkey, Ankara, Abstr, p. 247-248.

Toprak, V. (1994). Central Kızılırmak Fault Zone: Northern margin of Central Anatolian Volcanics, Turkish Journal of Earth Sciences,3,29-38.

Toprak, V., Göncüoğlu, M.C. (1993). Tectonic control on the development of Neogene-Quaternary Central Anatolian Volcanic Province, Turkey: Geological Journal, 28, 357-369.

Tuccimei, P., Giordano, G., Tedeschi, M. (2006). CO_2 release variations during the last 2000 years at the Colli Albani volcano (Roma, Italy) from speleothems studiesEarth and Planetary Science Letters, 243, 449-462.

Türkecan, A., Kuzucuoğlu, C., Mouralis, D., Pastre, J-F., Atıcı, Y., Guillou, H., Fontugne, M. (2004). Upper Pleistocene volcanism and palaeogeography in Cappadocia, Turkey, MTA-CNRS-TÜBİTAK 2001–2003 research programme. Project no:101Y109, MTA report no. 10652, 180 pp.

Uysal, I.T., Feng, Y., Zhao, J., Işık, V., Nuriel, P., Golding, S.D. (2009). Hydrothermal CO_2 degassing in seismically active zones during the late Quaternary. Chemical Geology 826 265, 442-454.

Uysal, I.T., Feng, Y., Zhao, J-X., Altunel, E., Weatherley, D., Karabacak, V., Cengiz, O., Golding, S.D, Lawrance, M.G., Collerson, K.D. (2007). U-series dating and geochemical tracing of late Quaternary travertine in co-seismic fissures, Earth and Planetary Science Letters, 257, 450-462.

Uysal, I.T., Feng, Y.-X., Zhao, J.-X., Bolhar, R., Isik, V., Baublys, K.A., Yago, A., Golding, S.D. (2011). Seismic cycles recorded in late Quaternary calcite veins: geochronological, geochemical and microstructural evidence, Earth and Planetary Science Letters, 303, 84–96.

Uysal, I.T., Ünal-İmer, E., Shulmeister, J., Zhao, J-X., Karabacak, V., Feng, Y.-X., Bolhar, R. (2019). Linking CO_2 degassing in active fault zones to long-term changes in water balance and surface water circulation, an example from SW Turkey, Quaternary Science Reviews, 214, 164-177.

Ünal-İmer, E., Uysal, I.T., Zhao, J.X., Işık, V., Shulmeister, J., İmer, A., Feng, Y.X. (2016). CO2 outburst events in relation to seismicity: constraints from micro-scale geochronology and geochemistry of late Quaternary vein carbonates, SW Turkey, Geochimica et Cosmochimica Acta, 187, 21–40.

Vermeesch, P. (2012). On the visualisation of detrital age distributions. Chemical Geology, v.312-313, 190-194.

Wang, C.-Y., Wang, C.H., Kuo, C.-H. (2004). Temporal change in groundwater level following the 1999 (Mw = 7.5) Chi-Chi earthquake, Taiwan, Geofluids, 4, 210-220.

Weinstein, Y., Nuriel, P., Inbar, M., Jicha, B.R., Weinberger, R. (2020). Impact of the Dead Sea Transform Kinematics on Adjacent Volcanic Activity, Tectonics, 39, 1, e2019TC005645

Williams, R.T., Goodwina, L.B., Sharpb, W.D., Mozley, P.S. (2017). Reading a 400,000-year record of earthquake frequency for an intraplate fault, Proceedings of the National Academy of Sciences, 114, 4983-4898.

Yıldırım, G., Mutlu, H., Karabacak, V., Uysal, I.T, Dirik, K., Temel, A., Yüce, G., Zhao, J-X. (2020). Temporal changes in geochemical-isotopic systematics of the late Pleistocene Akkaya travertines (Turkey) - Implications for fluid flow circulation and seismicity, Chemie der Erde (Geochemistry), doi: 10.1016/j.chemer.2020.125630

Zhao, J.-X., Hu, K., Collerson, K.D., Xu, H. (2001) Thermal ionization mass spectrometry U-series dating of a hominid site near Nanjing, China, Geology, 29, 27–30.

Zobin, V.M. (2003). Introduction to Volcanic Seismology (Vol. 6 of Developments in Volcanology). Amsterdam: Elsevier.

Figure Captions

Figure 1. a. Generalized tectonic setting of the Anatolian Block (yellow arrows show the plate motions). b. Shaded relief map of the Central Anatolian Volcanic Province (generated using the WorldImagery data merged to SRTM-3arc-second resolution digital data) (black lines show the Quaternary faults, blue circles show

Neogene activity while the yellow circles show Quaternary activity on stratovolcanoes). B: Balkaya site, S: Sarıhıdır site, I: Ihlara site.

Figure 2. Geological setting of the study area and locations of the travertine sites (simplified from Köksal and Göncüoğlu, 1997; Koçyiğit and Doğan, 2016 and authors' field observations) (base map is taken from GoogleEarth). Red line indicates the trace of the faults.

Figure 3. A representative thin section from the carbonates (sample A-2, location 4, Balkaya). The discontinuities in between the bands (hiatus) are noticeable (yellow lines). Arrows show the elongation of calcite fabrics (red lines indicate microcrystalline, blue lines indicate macrocrystalline) (right image is cross-polarized, while the image at the left is plane-polarized). Note that, we drilled preferentially microcrystalline parts for dating.

Figure 4. a. PAAS normalized NTE+Y patterns of Balkaya and Sarıhıdır carbonate samples and host rocks (Taylor and Mclennan, 1985) (host rock data from Toksoy-Köksal et al., 2008). b. δ 18O vs. δ 13C systematics for Balkaya and Sarıhıdır carbonate samples (blue cross: location 1, red cross: location 2, red circle: location 3, blue circle: location 4).

Figure 5. Comparison of oxygen isotope data on Balkaya carbonate veins with various climate records. Marine benthic record (Lisiecki and Raymo, 2005), Soreq cave, Israel (Bar-Matthews et al., 2003), Antro del Corchia cave, Italy (Drysdale et. al, 2005), Buraca Gloriosa cave, Portugal (Denniston et al., 2018), Kesang cave, China (Cheng et al., 2012).

Figure 6. Model on correlations of carbonate veins with the paleo-eruption records in the meaning of fractural positioning to the eruption centers in CAVP. B: Balkaya travertine site, S: Sarıhıdır travertine site, I: Ihlara travertine site.

Table Captions

Table 1. The cycle of episodic carbonate vein (banded) precipitation in tectonically active areas: fluid-rock interaction (modified from Karabacak et al., 2019).

Table 2. Geochronologic and stable isotope data.

Table 3. Comparison between the carbonate ages investigated in the study area and the volcanic eruption events in the surrounding region from the literature.

Figures.

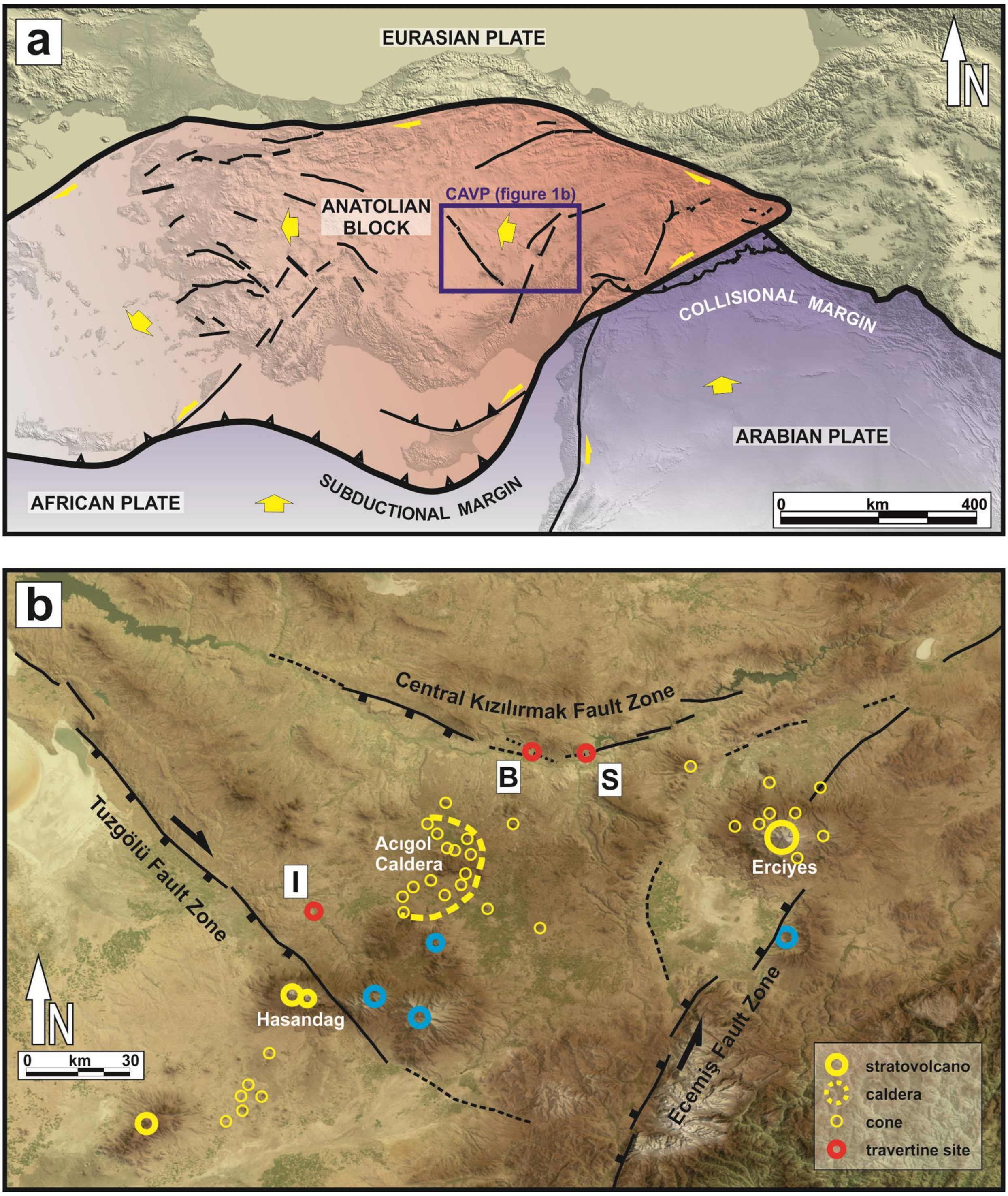
a
EURASIAN PLATE
ANATOLIAN BLOCK
CAVP (figure 1b)
COLLISIONAL MARGIN
ARABIAN PLATE
AFRICAN PLATE
SUBDUCTIONAL MARGIN
0 km 400
N
b
Central Kızılırmak Fault Zone
B
S
Tuzgölü Fault Zone
Acıgol Caldera
I
Erciyes
Hasandag
Ecemiş Fault Zone
0 km 30
N
stratovolcano
caldera
cone
travertine site

Figure 1

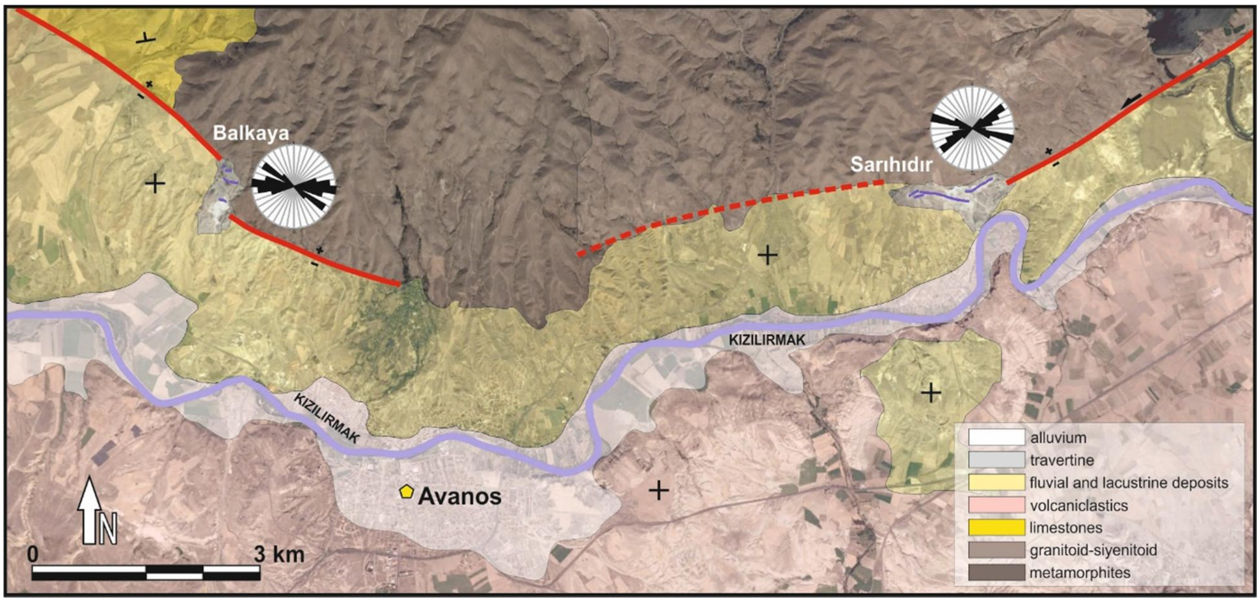
Balkaya
Sarıhıdır
KIZILIRMAK
KIZILIRMAK
Avanos
N
0
3 km
alluvium
travertine
fluvial and lacustrine deposits
volcaniclastics
limestones
granitoid-siyenitoid
metamorphites

Figure 2.

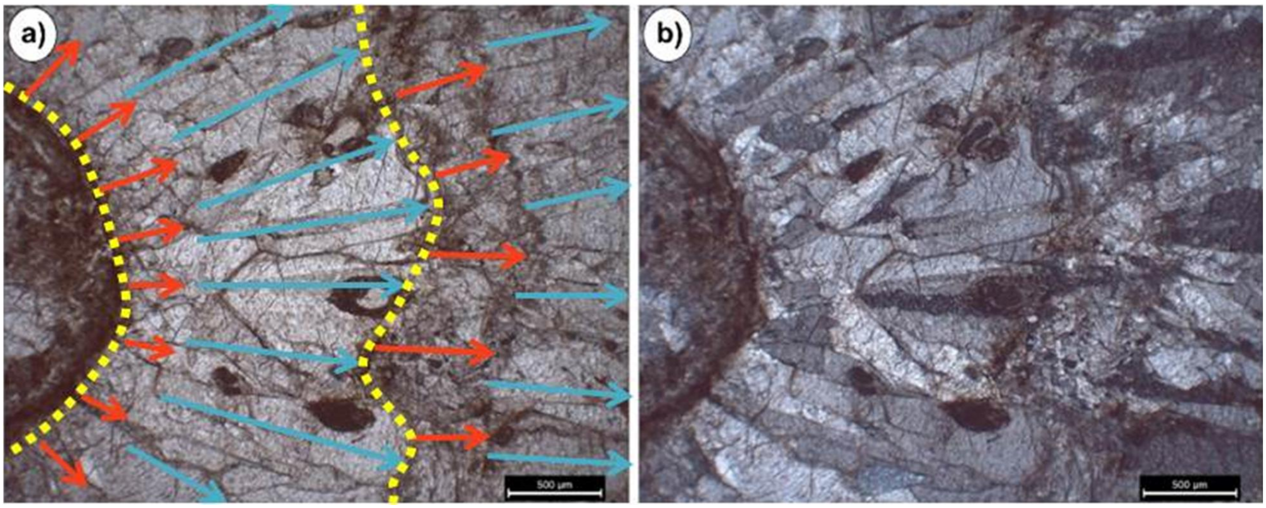

Figure 3.

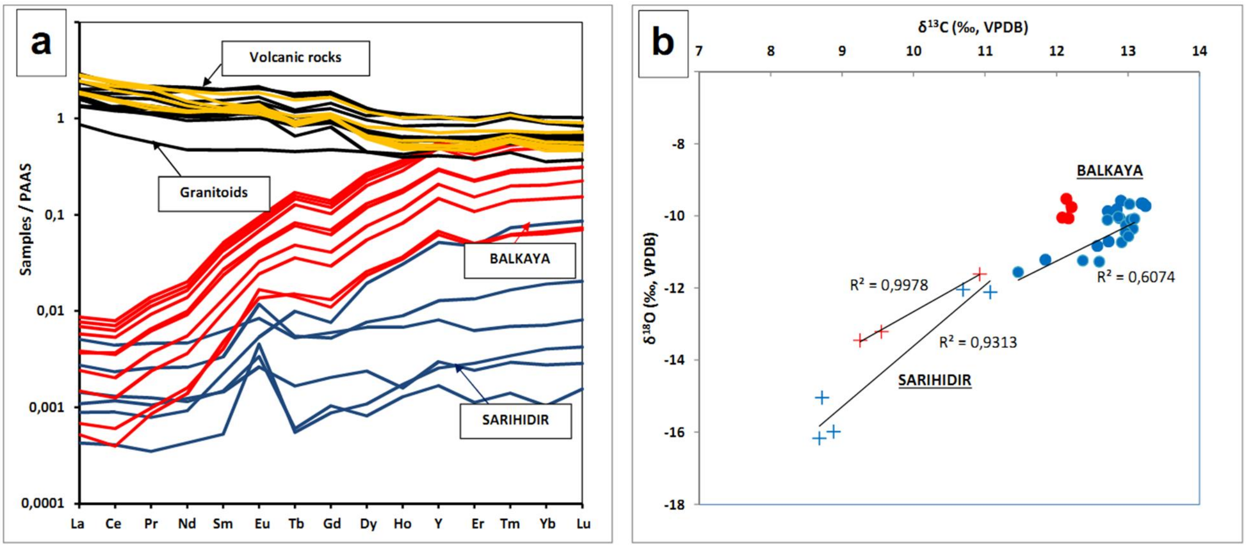
a
Volcanic rocks
Granitoids
BALKAYA
SARIHIDIR
Samples / PAAS
La
Ce
Pr
Nd
Sm
Eu
Tb
Gd
Dy
Ho
Y
Er
Tm
Yb
Lu
b
δ13C (‰, VPDB)
δ18O (‰, VPDB)
R² = 0,9978
R² = 0,9313
R² = 0,6074
BALKAYA
SARIHIDIR

Figure 4.

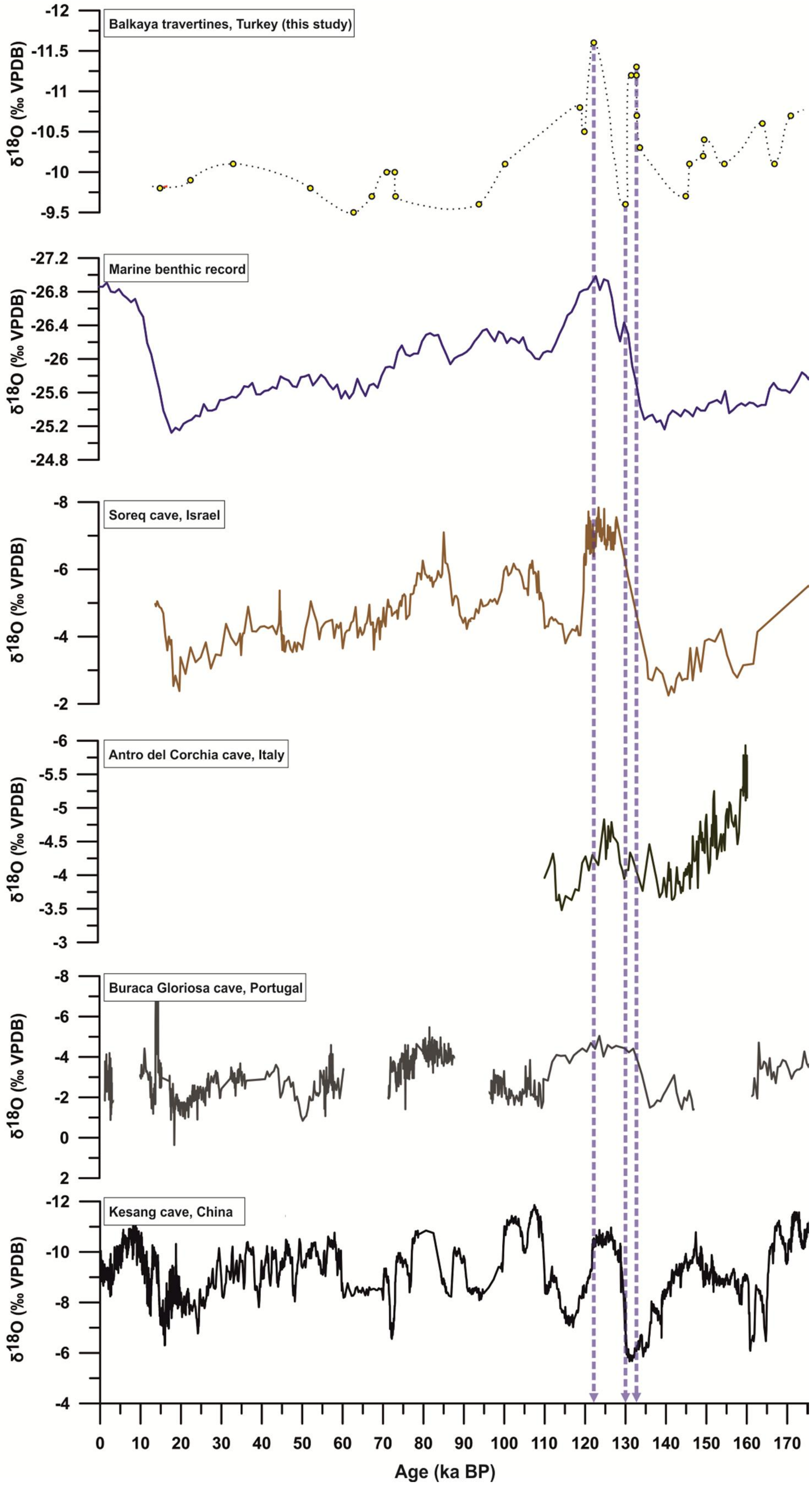
Balkaya travertines, Turkey (this study)
Marine benthic record
Soreq cave, Israel
Antro del Corchia cave, Italy
Buraca Gloriosa cave, Portugal
Kesang cave, China
δ18O (‰ VPDB)
Age (ka BP)

Figure 5.

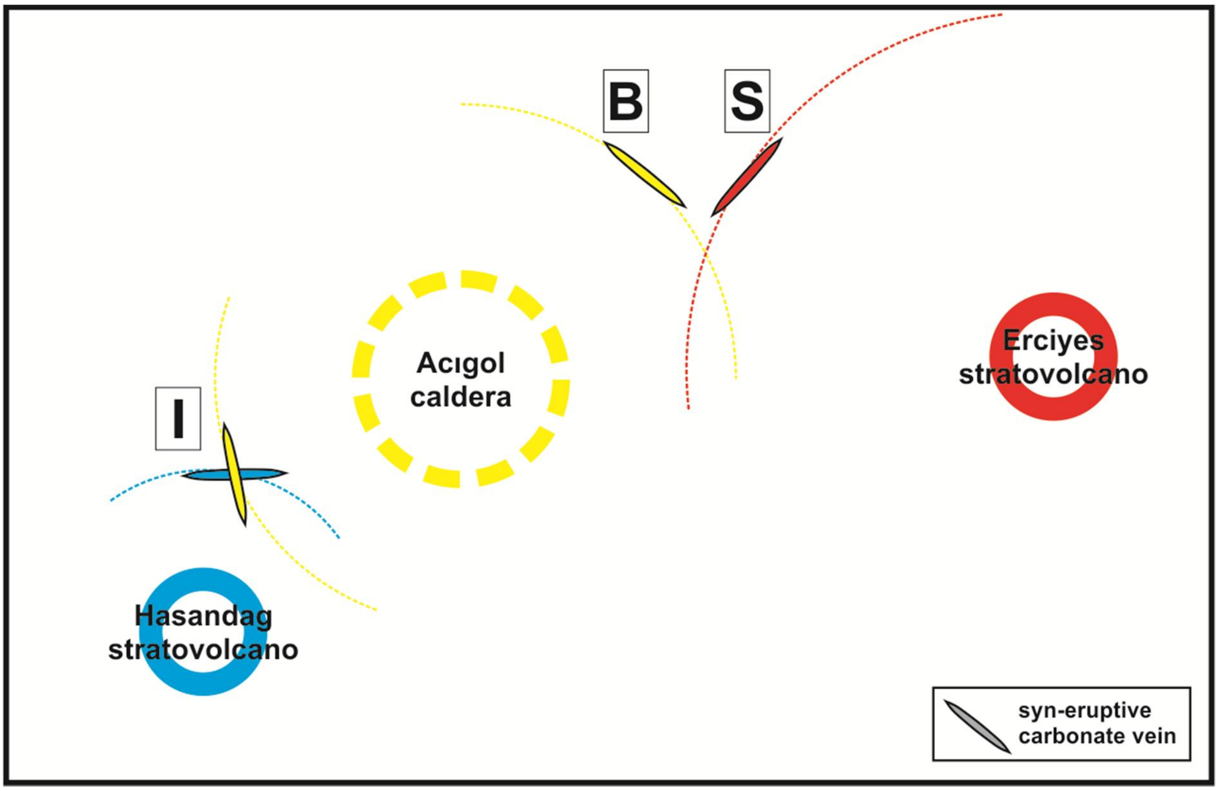
B
S
Acıgol
caldera
Erciyes
stratovolcano
I
Hasandag
stratovolcano
syn-eruptive
carbonate vein

Figure 6.

Table 1. The cycle of episodic carbonate vein (banded) precipitation in tectonically active areas: fluid-rock interaction (modified from Karabacak et al., 2019).

<table>
<tr><th>period</th><th>event</th><th colspan="2">result</th><th>evidence</th></tr>
<tr><td rowspan="2">coseismic</td><td>seismic release</td><td colspan="3">opening/reopening of fractures</td></tr>
<tr><td>simultaneous fluid circulation in fracture systems and expulsion of depressurized/supersaturated hot water</td><td rowspan="2">single carbonate band</td><td>rapid precipitation of banded carbonate on both walls of the fracture (planar)</td><td>whitish microcrystalline calcite that is related to abundant fluid inclusions with high-CO_2 degassing</td></tr>
<tr><td>postseismic</td><td>saturated but relatively slow fluid flow</td><td>plugging of the fracture along the carbonate vein</td><td>light-transparent macrocrystalline calcites that are precipitated at slow degassing rates during the time up to sealing</td></tr>
<tr><td>interseismic</td><td>unsaturated and slow fluid flow</td><td colspan="2">shifting spring points (pipes) along the sealed fracture</td><td>hiatus (no precipitation)</td></tr>
</table>

Table 2. Geochronologic and stable isotope data.

site	location	sample	corr. age (ka)	±2s	$\delta^{13}C$ (VPDB)	$\delta^{18}O$ (VPDB)	$\delta^{18}O$ (VSMOW)
SARIHIDIR	1	01	29	50	10,7	-12,0	18,5
		02	8,4	5,7	8,9	-16,0	14,5
		03	11,3	6,0	8,7	-15,0	15,5
		04	8,8	3,8	8,7	-16,2	14,3
		05	7,5	9,8	11,1	-12,1	18,4
	2	06-1	82	121	9,3	-13,4	17,1
		06-2	66	39	10,9	-11,6	18,9
		06-3	81	16	9,5	-13,2	17,3
BALKAYA	3	11A	52,1	8,4	12,2	-9,8	20,7
		11B	62,8	8,4	12,1	-9,5	21,0
		12C	33	10	12,2	-10,1	20,4
		12D	73	13	12,1	-10,0	20,5
	4	A-1	67,3	5,6	13,2	-9,7	20,8
		A-2	14,9	3,2	12,8	-9,8	20,7
		B	22,4	2,1	12,7	-9,9	20,6
		C-1	93,8	3,9	13,2	-9,6	20,9
		C-2	73,2	2,6	13,2	-9,7	20,8
		D-1	130,1	4,9	12,9	-9,6	20,9
		D-2	100,3	3,2	12,9	-10,1	20,4
		E--1	118,8	2,9	12,6	-10,8	19,7
		E--2	132,9	2,7	12,7	-10,7	19,8
		F	132,8	3,9	11,8	-11,2	19,3
		G-1	132,8	3,5	12,6	-11,3	19,2
		G-2	131,5	2,1	12,4	-11,2	19,3
		G-3	122,3	1,1	11,5	-11,6	18,9
		H-1	149,3	7,5	13,0	-10,2	20,3
		H-2	133,6	3,5	13,0	-10,3	20,2
		H-3	154,6	6,0	13,0	-10,1	20,4
		H-4	149,6	5,8	13,1	-10,4	20,1
		H-5	119,9	8,7	13,0	-10,5	20,0
		H-6	171	18	12,9	-10,7	19,8
		H-7	164	27	13,0	-10,6	19,9
		I-1	167	15	13,1	-10,1	20,4
		I-2	145	10	13,0	-9,7	20,8
		J-1	71	15	12,9	-10,0	20,5
		J-2	146	15	12,7	-10,1	20,4

Table 3. Comparison between the carbonate ages investigated in the study area and the volcanic eruption events in the surrounding region from the literature.

U-series age data of studied carbonates			volcanic events dated around the study area		
site	sample	corr. age (ka BP)	eruption date (ka BP)	eruption center and evidence	reference
BALKAYA	A-2	14,9±3,2	14	Acıgöl - sediment cores in the late Pleistocene Eski Acıgöl maar, tephra layer (radiocarbon)	Kuzucuoglu et al., 1998
			16	Acıgöl - Acıgöl maar (U-Th)	Roberts et al., 2001
	B	22,4±2,1	22,3±1,1	Acıgöl - Karnıyarık, rhyolitic lava nearly aphyric (U-Th/He)	Schmitt et al., 2011
	12c	33±10	32±3*	Acıgöl - south of Kocadağ (K-Ar)	Türkecan et al., 2004
	12d	73±13	75	Acıgöl – Taşkesik Hill, lava dome	Bigazzi et al., 1993
	C-2	73,2±2,6			
	C-1	93,8±3,9	93±2*	Acıgöl - Boğazköy (obsidian)	Türkecan et al., 2004
	D-2	100,3±3,2	96,0±13,0	Acıgöl - basaltic lava (Karnıyarık Hill) (Ar-Ar)	Doğan, 2011
	E-1	118,8±2,9	117±4	Acıgöl - Alacasar, rhyolitic pumice aphyric (U-Th/He)	Schmitt et al., 2011
	H-5	119,9±8,7			
	I-2	145±10	147±8*	Acıgöl – Taşkesik Hill, rhyolitic lava nearly aphyric (U-Th/He)	Schmitt et al., 2011
	J-2	146±15			
	H-1	149,3±7,5			
	H-4	149,6±5,8			
	H-7	164±27	163±7	Acıgöl - upper Acıgöl tuffs Boğazköy, rhyolitic pumice aphyric (U-Th/He)	Schmitt et al., 2011
	I-1	167±15			
SARIHIDIR	05	7,5±9,8	7,2±0,9	Erciyes - lava-flow (Karagüllü) (cosmogenic ^{36}Cl)	Sarıkaya et al., 2017
			7,7±0,4	Erciyes - lava-flow (Perikartın) (cosmogenic ^{36}Cl)	Sarıkaya et al., 2017
	02	8,4±5,7	8,8±0,6	Erciyes - lava-flow (Dikkartın) (cosmogenic ^{36}Cl)	Sarıkaya et al., 2017
	04	8,8±3,8			
	03	11,3±6,0	13±5	Erciyes - cinder cone basalt (K-Ar)	Doğan-Külahcı, 2015
	06-03	81±16	80±10	Erciyes - augite-hypersthene andesite, lava-flow (Karigtepe) (K-Ar)	Notsu et al., 1995
	06-01	82±121			

* the eruptions of Acıgöl caldera dated from carbonate veins of Ihlara travertine site (Karabacak et al., 2017).

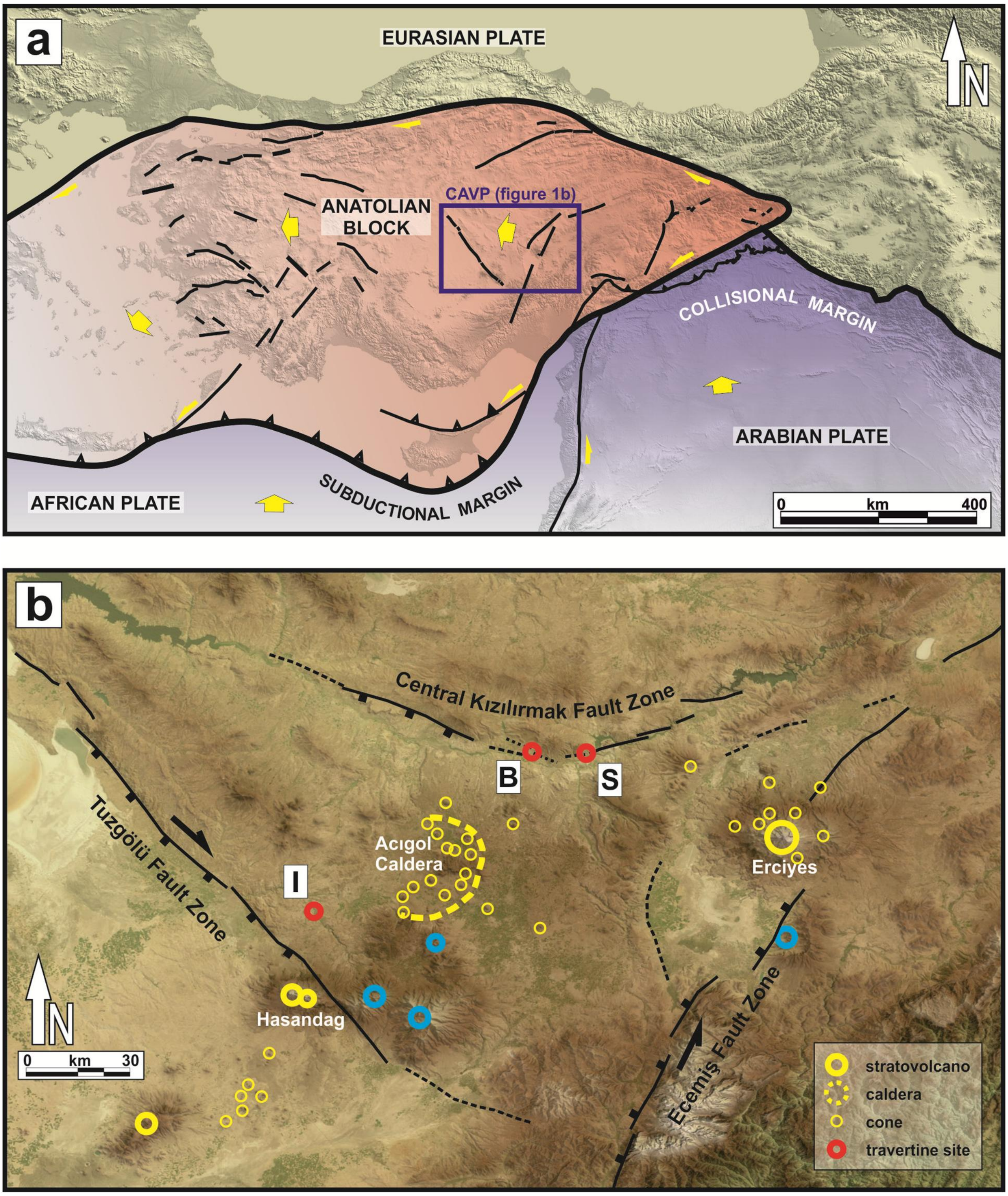
a
EURASIAN PLATE
ANATOLIAN BLOCK
CAVP (figure 1b)
COLLISIONAL MARGIN
ARABIAN PLATE
AFRICAN PLATE
SUBDUCTIONAL MARGIN
N
0 km 400
b
Central Kızılırmak Fault Zone
B
S
Tuzgölü Fault Zone
Acıgol Caldera
I
Erciyes
Hasandag
Ecemiş Fault Zone
N
0 km 30
stratovolcano
caldera
cone
travertine site

Figure 1

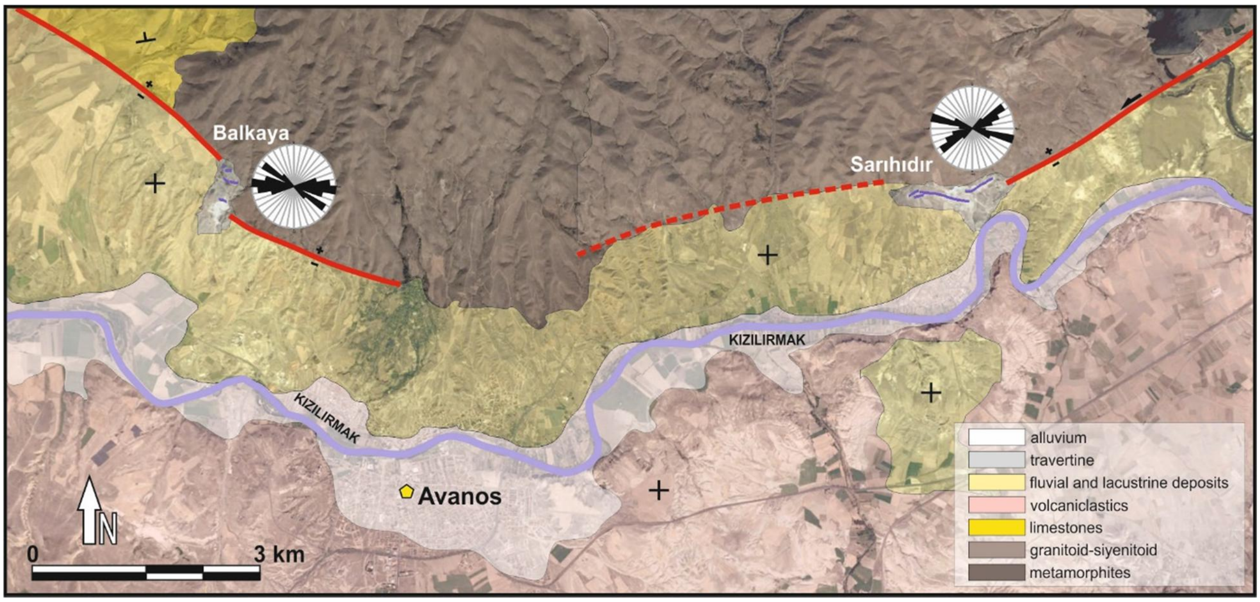
Balkaya
Sarıhıdır
KIZILIRMAK
KIZILIRMAK
Avanos
N
0
3 km
alluvium
travertine
fluvial and lacustrine deposits
volcaniclastics
limestones
granitoid-siyenitoid
metamorphites

Figure 2.

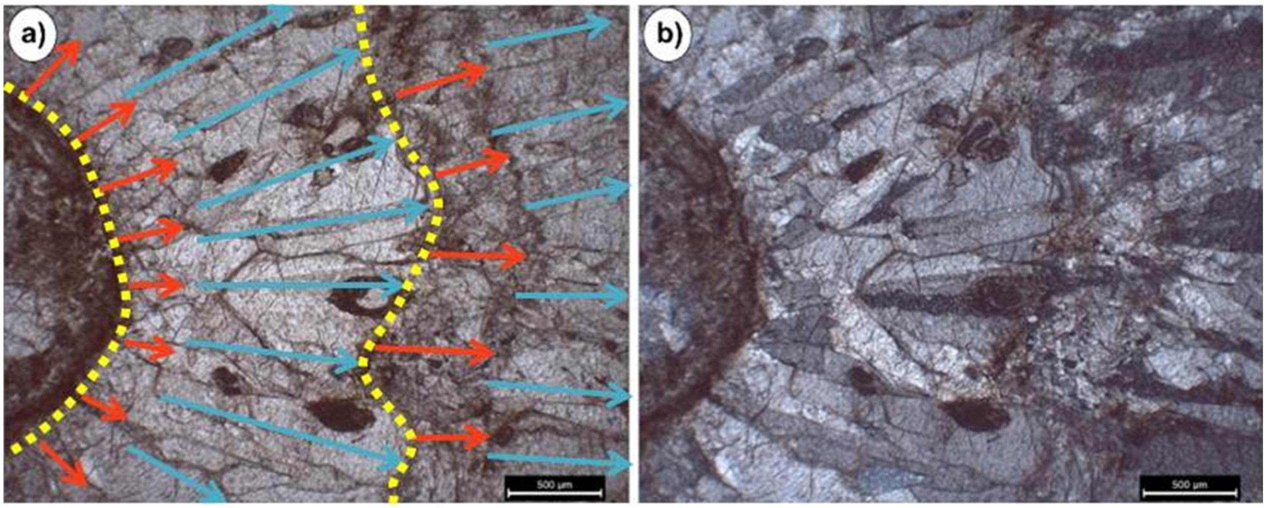

Figure 3.

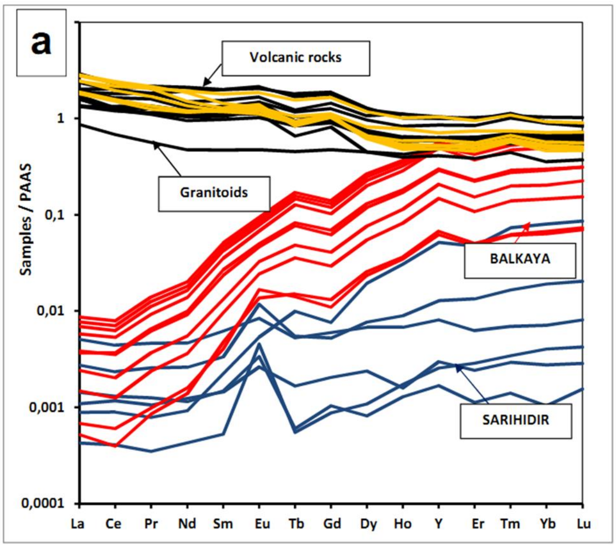
a
Volcanic rocks
Granitoids
BALKAYA
SARIHIDIR
Samples / PAAS
1
0,1
0,01
0,001
0,0001
La
Ce
Pr
Nd
Sm
Eu
Tb
Gd
Dy
Ho
Y
Er
Tm
Yb
Lu

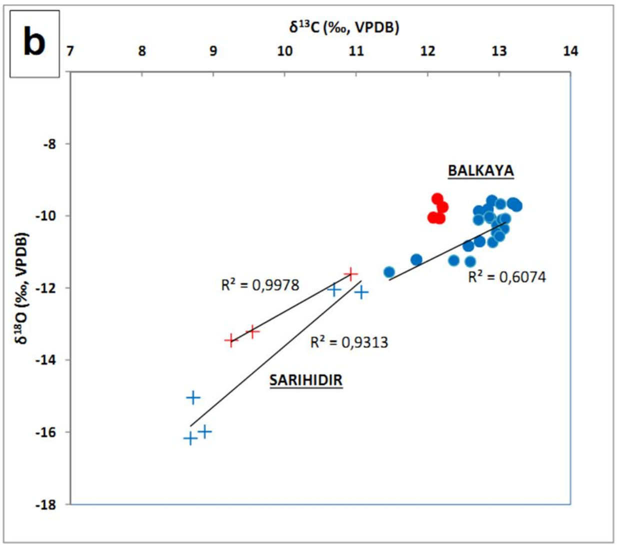
b
δ13C (‰, VPDB)
7
8
9
10
11
12
13
14
δ18O (‰, VPDB)
-8
-10
-12
-14
-16
-18
BALKAYA
SARIHIDIR
R² = 0,9978
R² = 0,9313
R² = 0,6074

Figure 4.

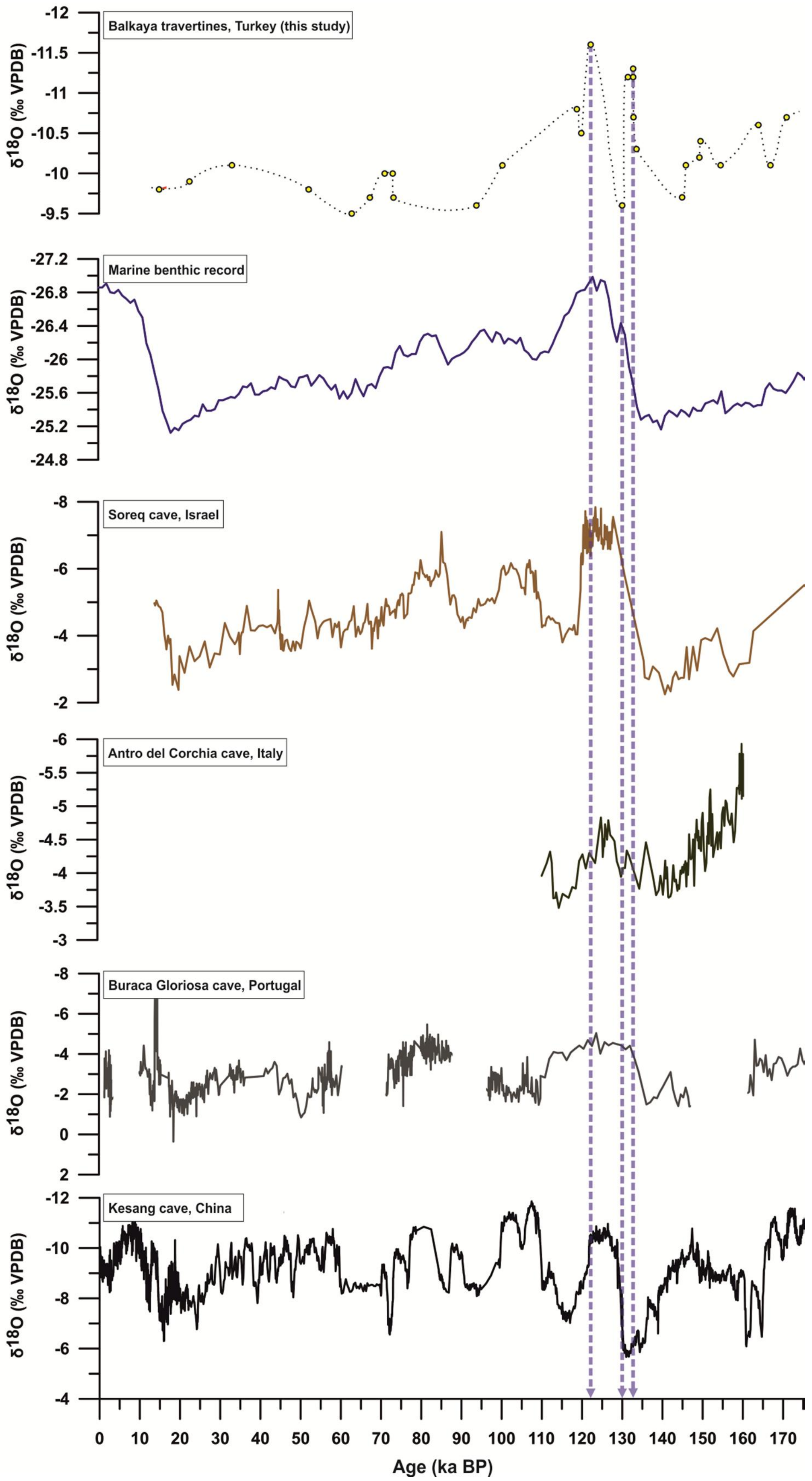

Balkaya travertines, Turkey (this study)
Marine benthic record
Soreq cave, Israel
Antro del Corchia cave, Italy
Buraca Gloriosa cave, Portugal
Kesang cave, China
δ18O (‰ VPDB)
Age (ka BP)

Figure 5.

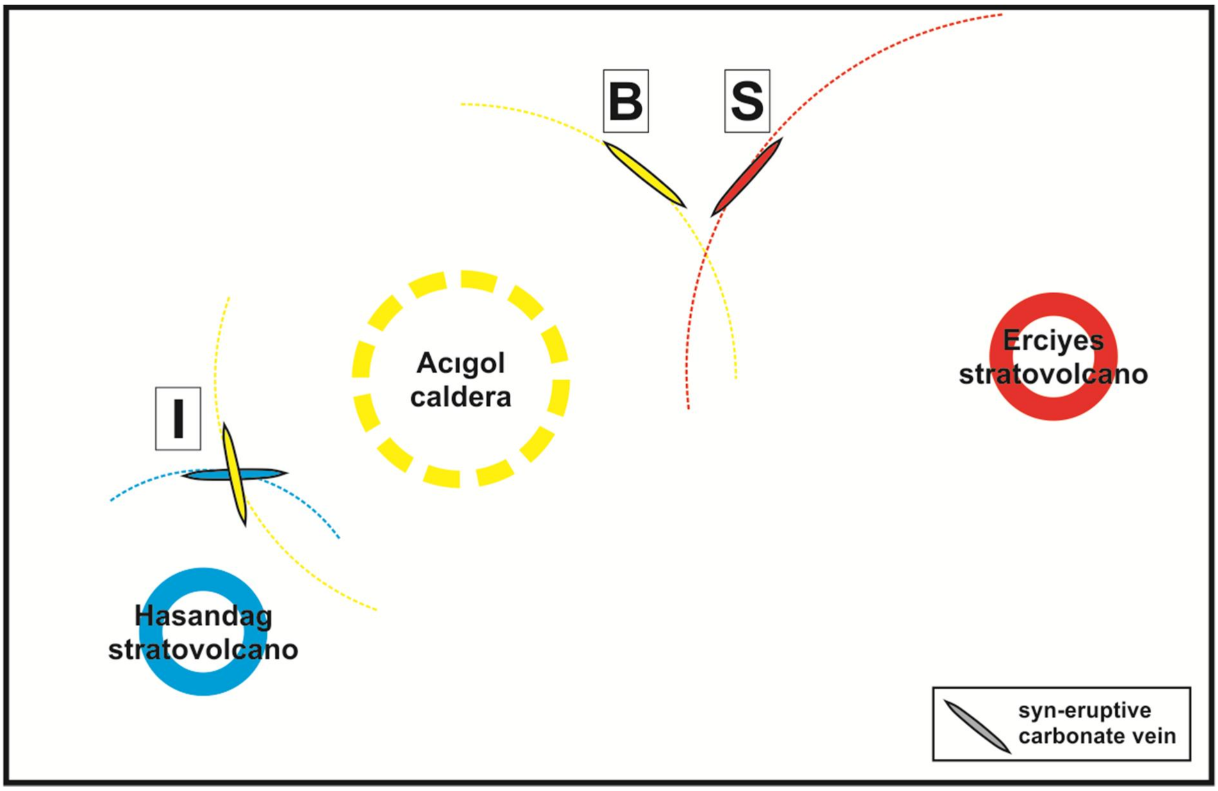
B
S
Acıgol
caldera
Erciyes
stratovolcano
I
Hasandag
stratovolcano
syn-eruptive
carbonate vein

Figure 6.

Tectonics

Supporting Information for

Manifestations of syn-eruptive fluid circulations on carbonate veins, Central Anatolian Volcanic Province

Volkan Karabacak (1), Halim Mutlu (2), Kıymet Deniz (2)

(1) Department of Geological Engineering, Eskisehir Osmangazi University, Turkey (karabacak@ogu.edu.tr)

(2) Department of Geological Engineering, Ankara University, Turkey

Contents of this file

Figures S1 to S11

Tables S1 to S6

Introduction

This information includes supplementary figures and tables for sampling sites, results of sample analyses, and volcanic eruption records.

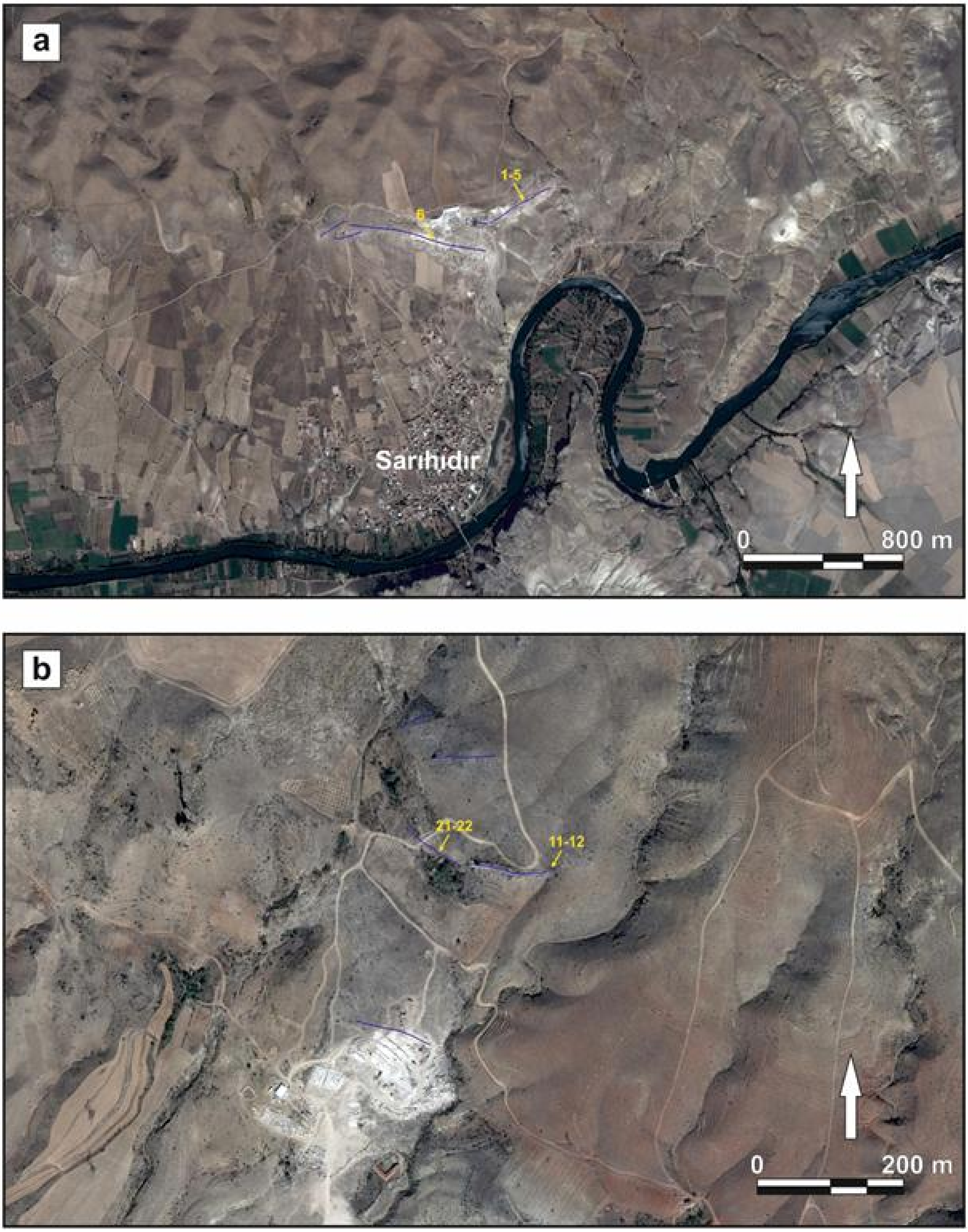

Figure S1. Satellite views of the carbonate veins and sampling locations (taken from Google Earth). a. Sarıhıdır site, b. Balkaya site.

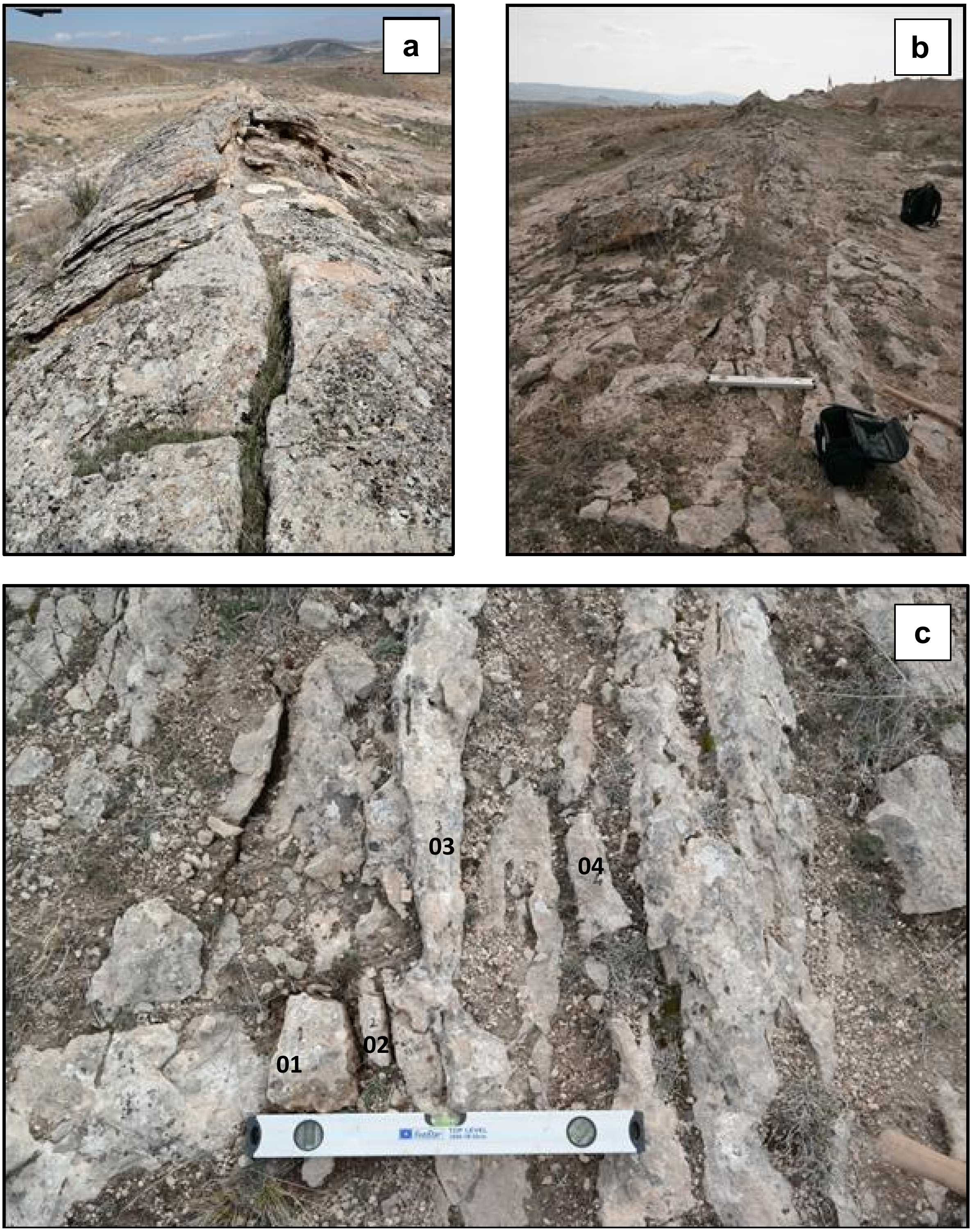

Figure S2. Field views of the sampling location L1, Sarıhıdır. **a.** Well-protected morphology of the fissure ridge. **b.** Carbonate vein along the fissure ridge and **c.** collected samples.

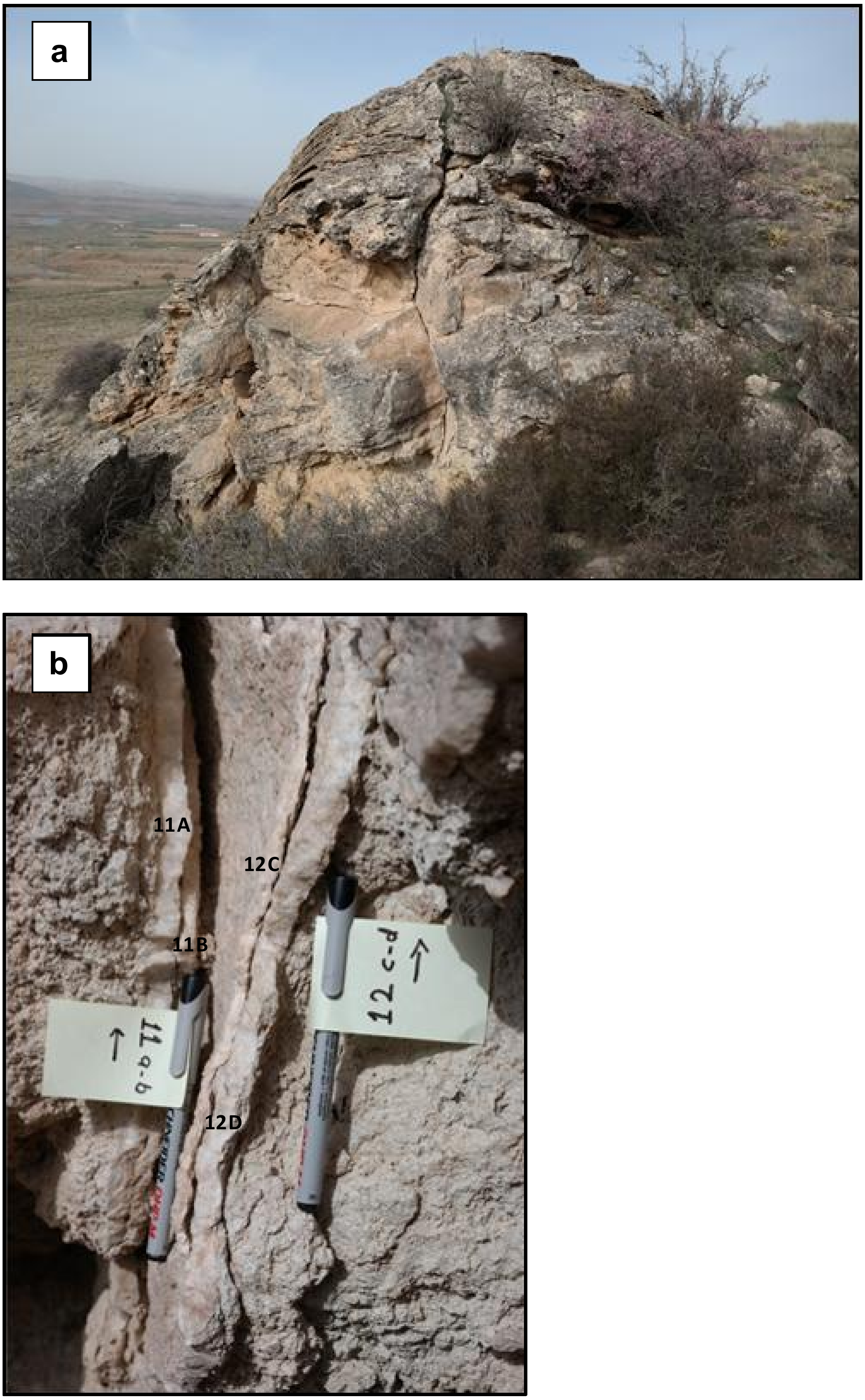

Figure S3. Field views of the sampling location L3, Balkaya. **a.** Well-protected morphology of the fissure ridge. **b.** Carbonate vein along the fissure ridge and collected samples.

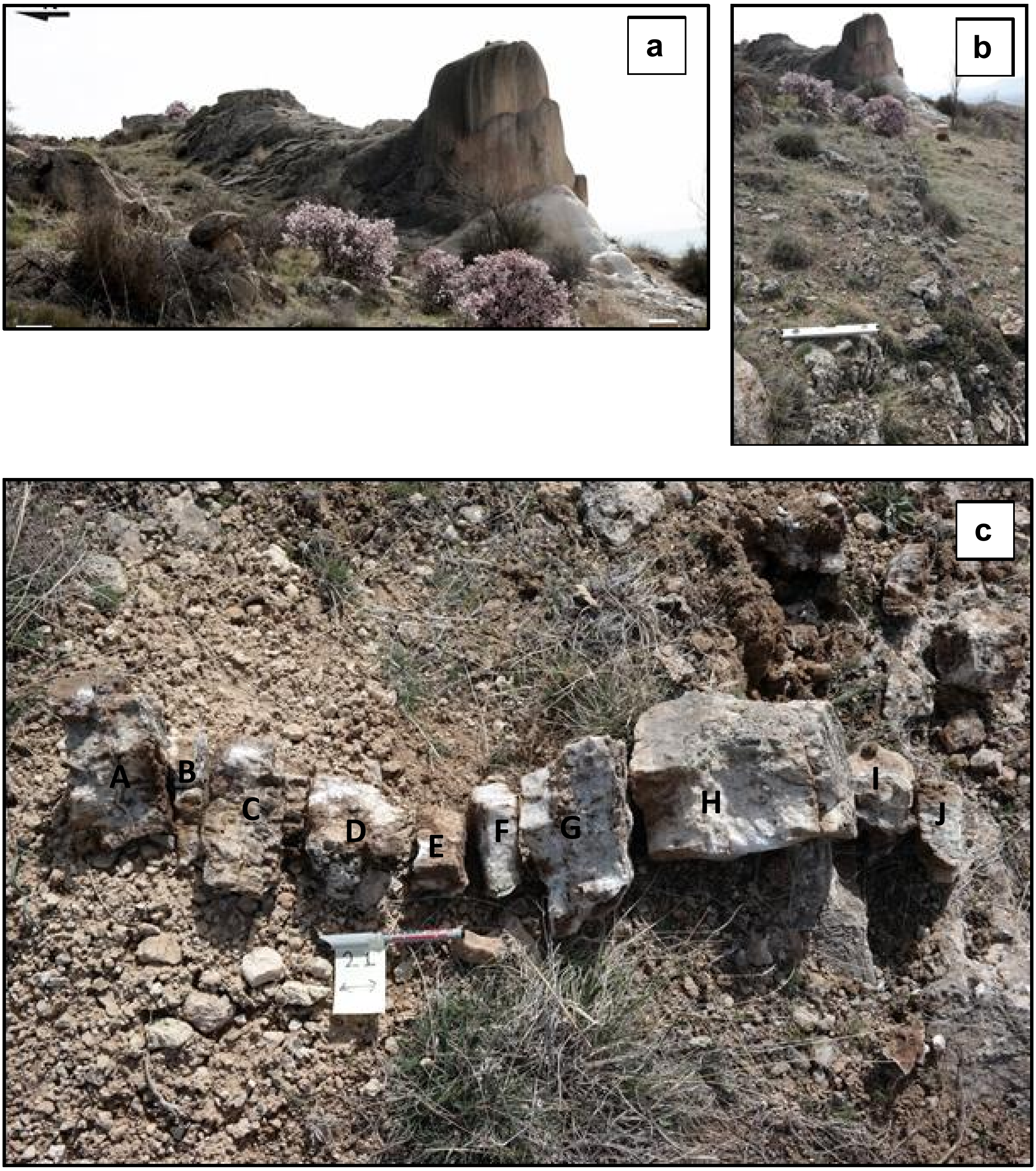

Figure S4. Field views of the sampling location L4, Balkaya. **a.** Well-protected morphology of the fissure ridge. **b.** Carbonate vein along the fissure ridge and **c.** collected samples.

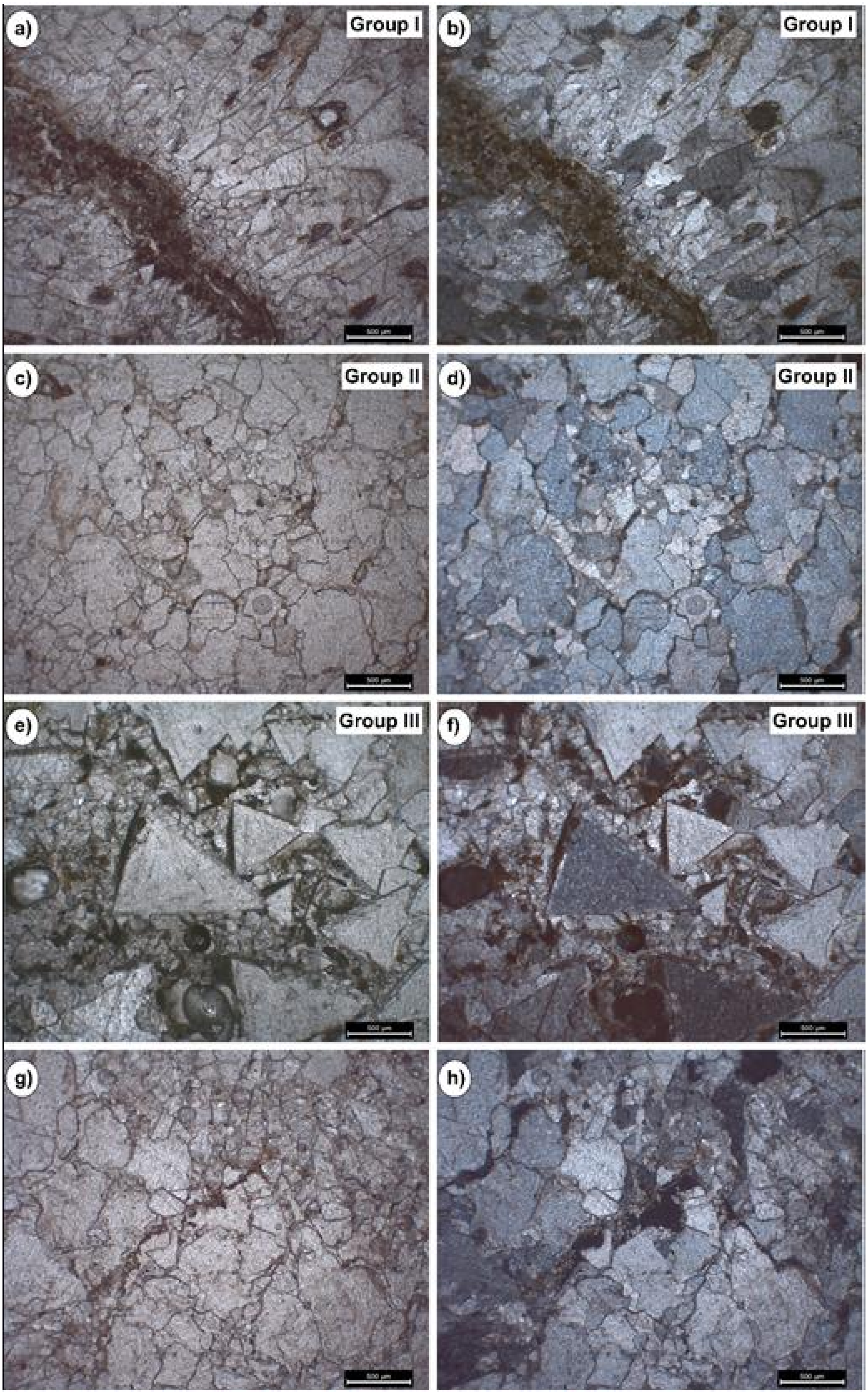

Figure S5. Representative thin section photos of the Balkaya samples. Photos at the right side are cross-polarized and those at the left are plane-polarized. a) and b) idiomorph, coarse crystalline, needle-shaped calcite minerals in sample A2; c) and d) mosaic texture in sample J1 showing various sized xenomorphic calcites; e) and f) flow and granular textures with shelter porosity in sample H5; g) and h) fine crystalline granular texture with shelter and fenestral porosity in sample J1.

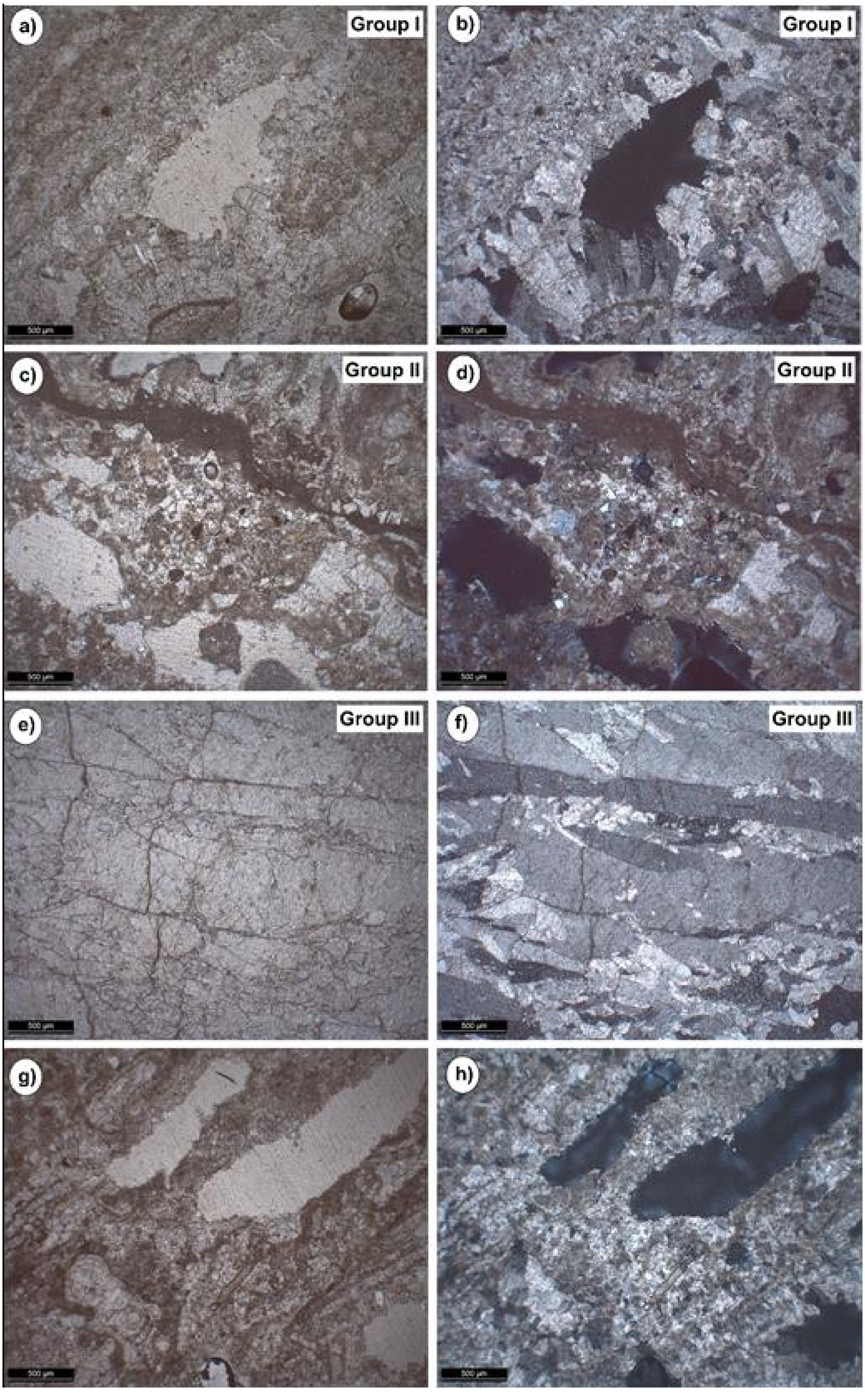

Figure S6. Representative thin section photos of the Sarıhıdır samples. Photos at the right side are cross-polarized and those at the left are plane-polarized. a) and b) fine to coarse crystalline calcite with rare quartz, pyroxene, epidote and clay minerals in sample 01; c) and d) finely crystalline granular texture and shelter type porosity in sample 03; e) and f) very finely banded and well developed flow texture with shelter and fenestral type porosity in sample 04; g) and h) clay minerals in the carbonate bands of sample 01.

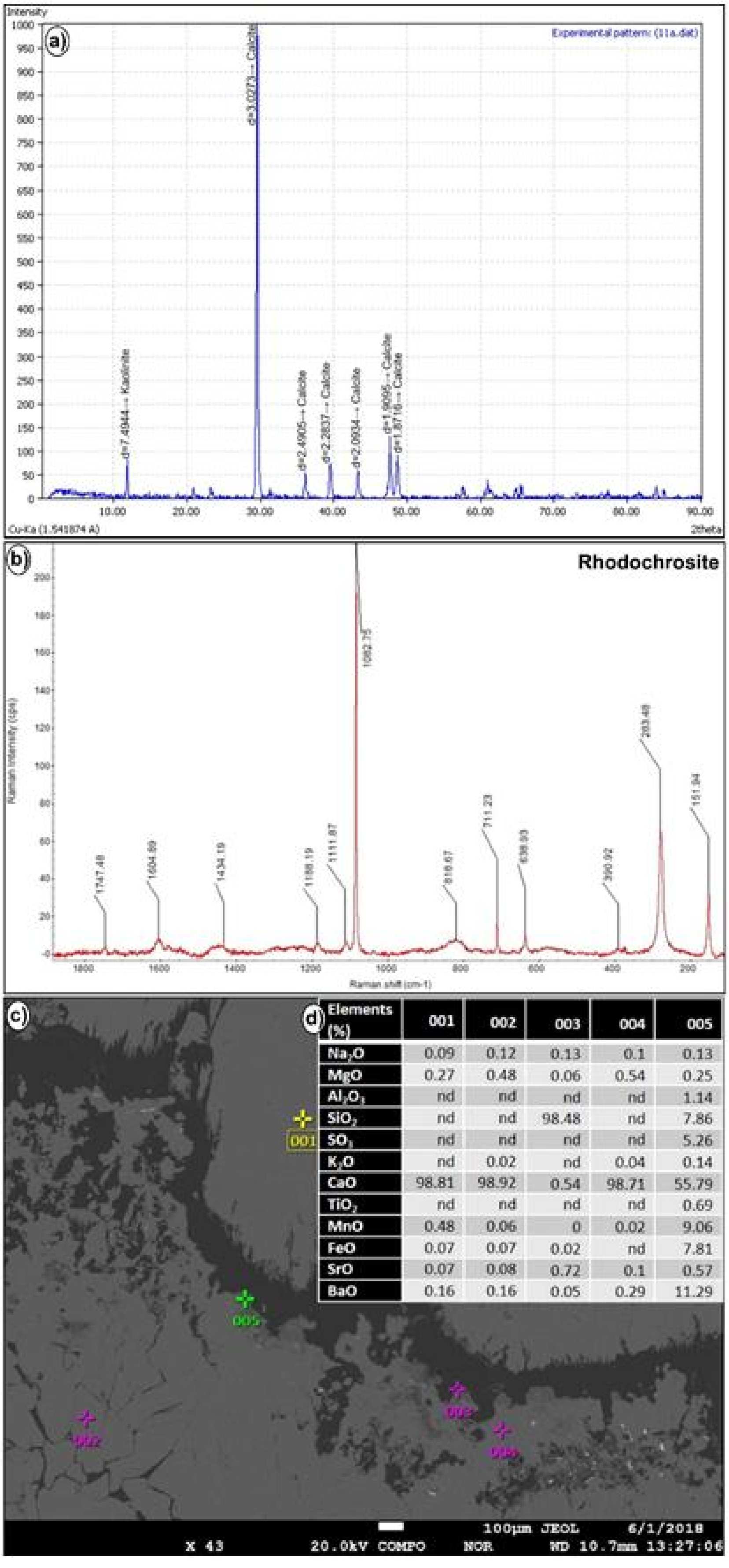

Elements (%)	001	002	003	004	005
Na_2O	0.09	0.12	0.13	0.1	0.13
MgO	0.27	0.48	0.06	0.54	0.25
Al_2O_3	nd	nd	nd	nd	1.14
SiO_2	nd	nd	98.48	nd	7.86
SO_3	nd	nd	nd	nd	5.26
K_2O	nd	0.02	nd	0.04	0.14
CaO	98.81	98.92	0.54	98.71	55.79
TiO_2	nd	nd	nd	nd	0.69
MnO	0.48	0.06	0	0.02	9.06
FeO	0.07	0.07	0.02	nd	7.81
SrO	0.07	0.08	0.72	0.1	0.57
BaO	0.16	0.16	0.05	0.29	11.29

Figure S7. Representative (a) XRD (sample 11A), (b) CRS (A-2) and (c-d) EPMA (A-1) studies of samples from Balkaya site.

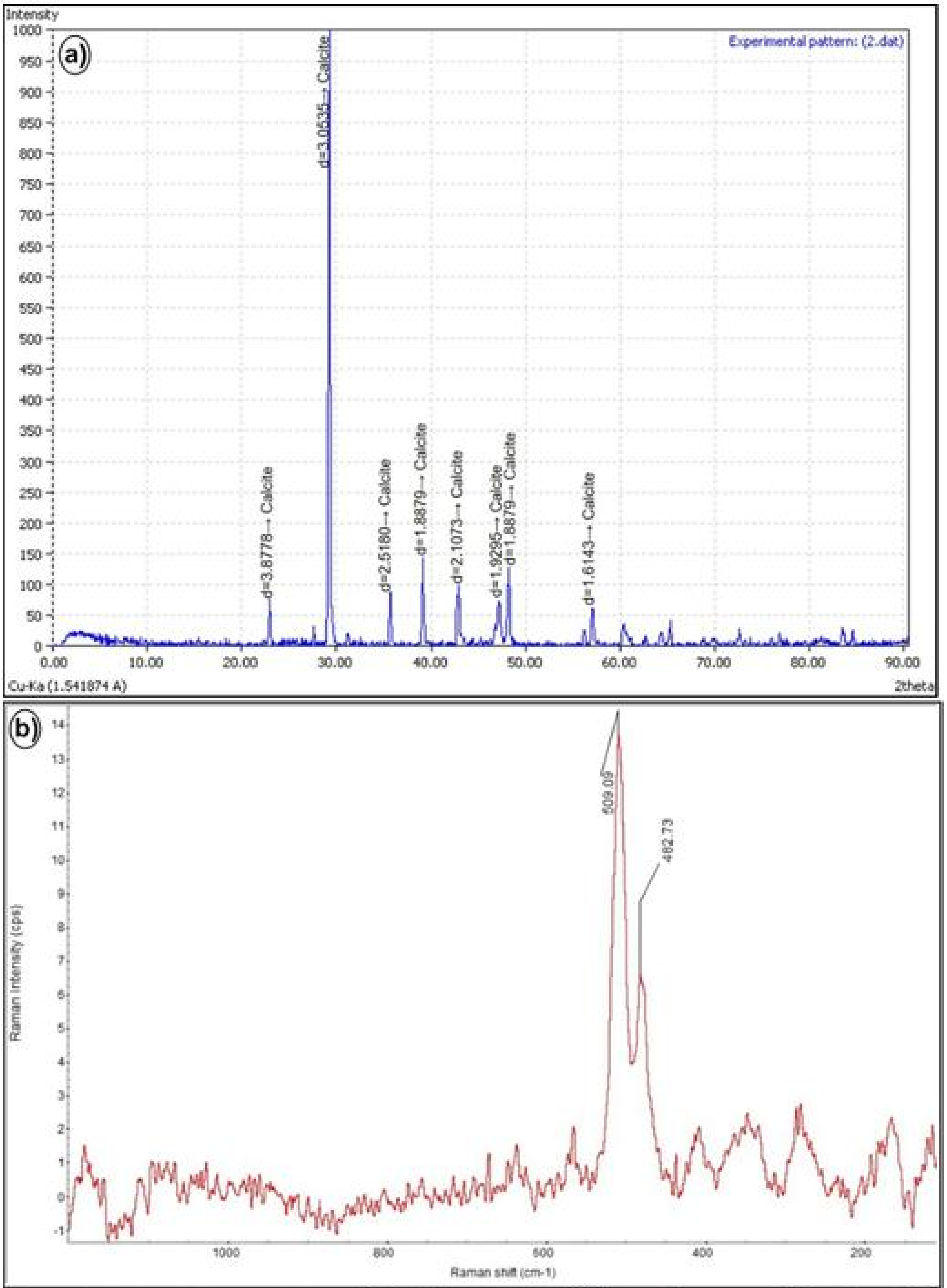

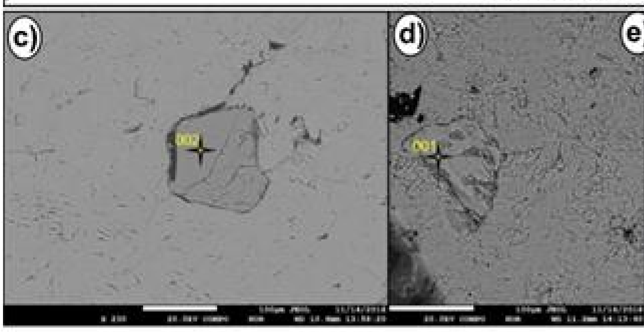

e)

Elements (%)	001 (Pyroxene)	002 (Epidote)
Na_2O	0.17	nd
SiO_2	52.35	57.91
MgO	15.67	0.01
Al_2O_3	3.11	27.81
MnO	0.15	0.05
K_2O	0.01	0.34
FeO	5.01	0.15
TiO_2	0.23	0.00
CaO	22.79	9.19
Total	100.16	95.46

Figure S8. Representative (a) XRD (sample 02), (b) CRS (sample 06-3) and (c-e) EPMA (sample 01) studies of samples from Sarıhıdır site.

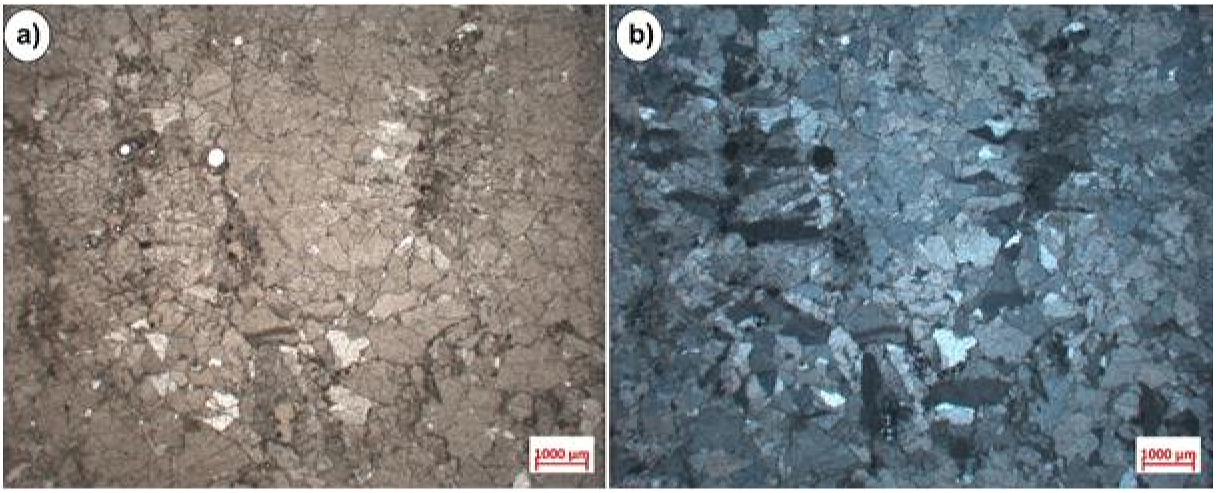

Figure S9. Thin section images of the Balkaya sample D1, which is dated at 130 ka; a) plane-polarized, b) cross-polarized.

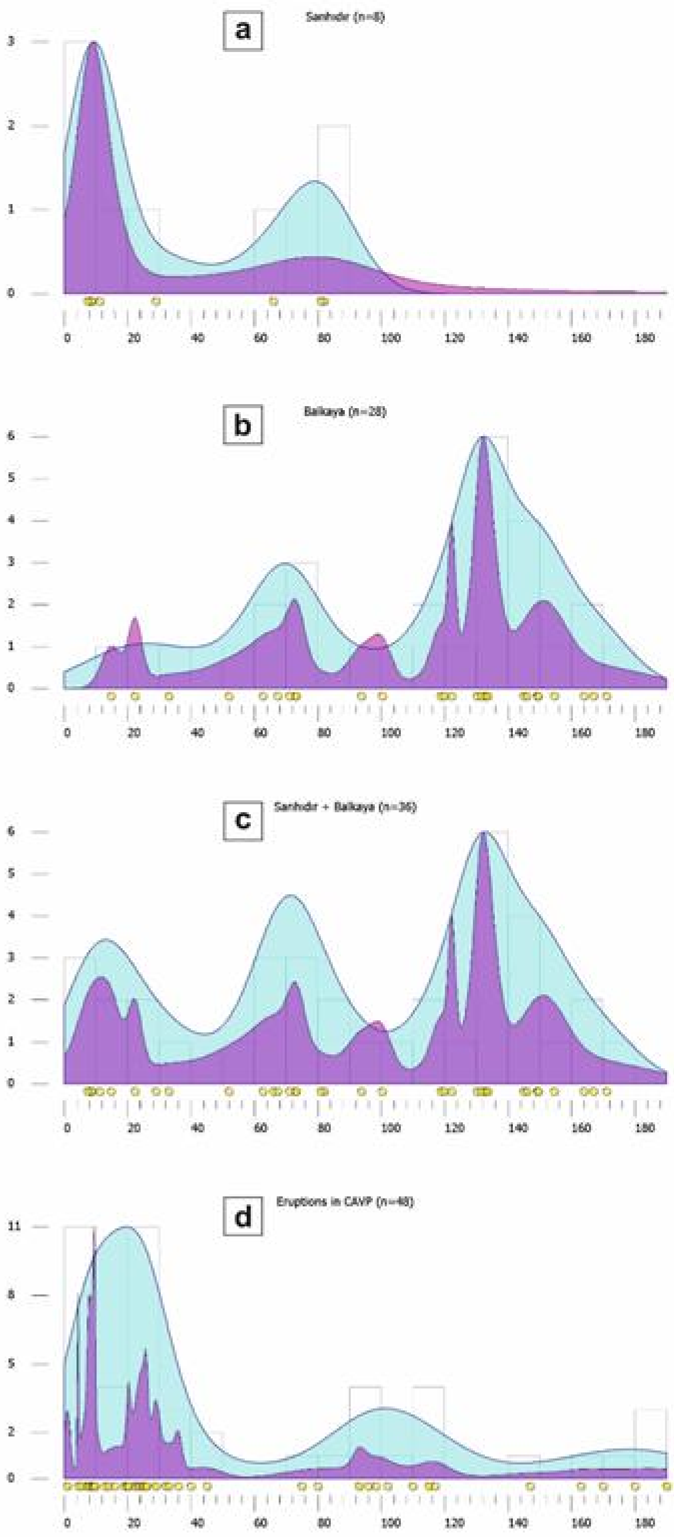

Figure S10. Relative probability curves of the U-series ages of carbonate samples and the previously dated paleo-eruptions. **a.** Sarıhıdır carbonate veins, **b.** Balkaya carbonate veins, **c.** the results of all carbonate samples, **d.** paleo-eruption records in literatures (Table S1) (purple plot: Probability density, light blue plot: Kernel density, rectangles: histograms of the samples). Note that x and y axes represent dating results in ka BP and number of samples respectively.

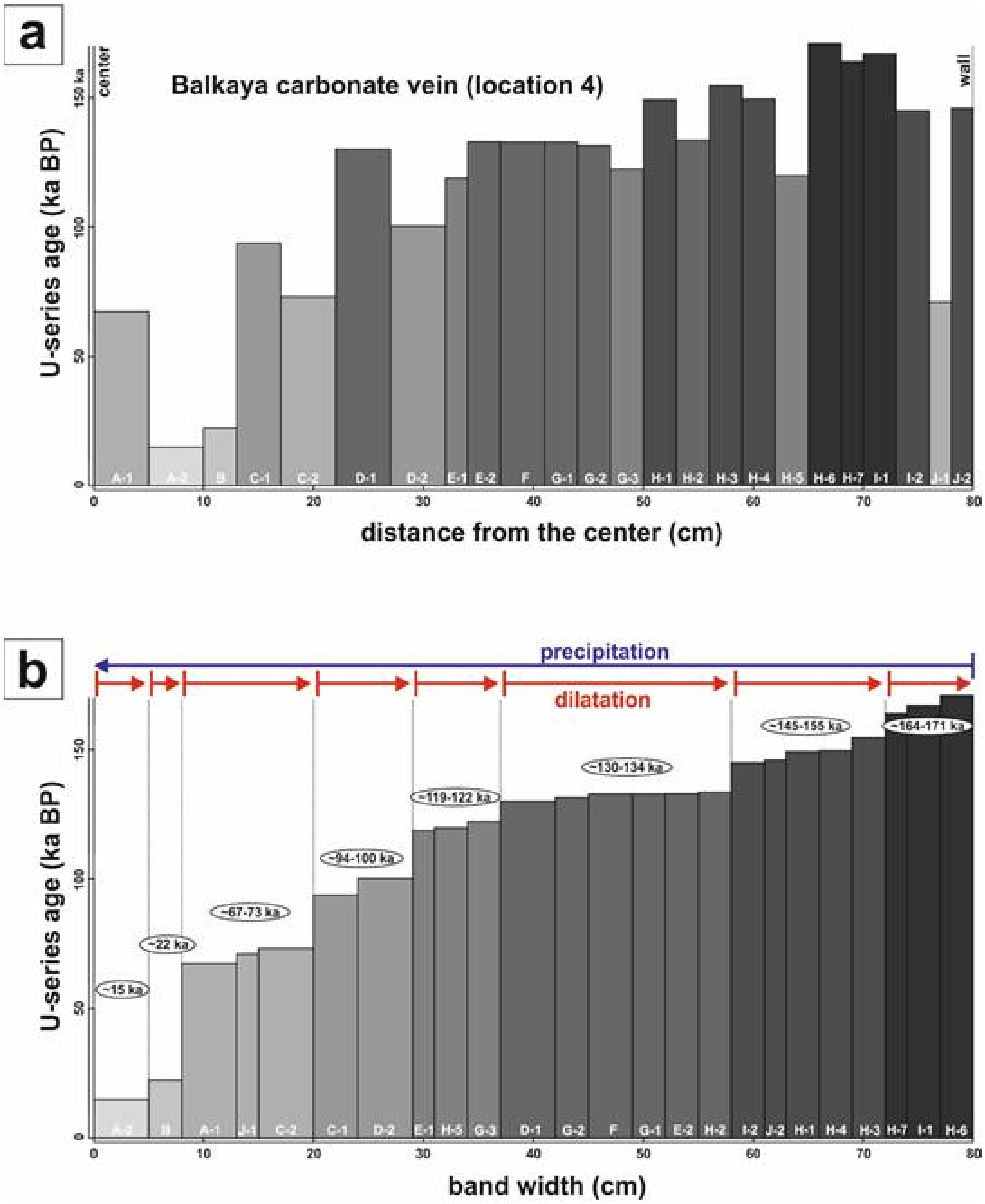

Figure S11. a. The U-series ages distribution of carbonate bands with respect to distance from the vein center to the wall on the L4-vein in Balkaya. Note that carbonate vein presents a continuous precipitation record. **b.** The graph is ordered as the coeval bands (U-series age vs. the band widths). Note that the vein has at least 8 rapid dilatation periods.

Table S1. Volcanic events dated in the last 190 ka around the study area.

	eruption date (ka BP)	eruption center	evidence	reference
1.	<1	Erciyes	basaltic lava (east of Hocalılar) (K-Ar)	Doğan-Külahcı, 2015
2.	<1	Erciyes	cinder cone lava-flow (south of Hacılar) (K-Ar)	Doğan-Külahcı, 2015
3.	4,4±0,2	Acıgöl	sediment cores in the late Pleistocene Eski Acıgöl maar, Tephra layer T17 (radiocarbon)	Kuzucuoglu et al., 1998
4.	5,5	Acıgöl	sediment cores in the late Pleistocene Eski Acıgöl maar, Tephra layer T15 (radiocarbon)	Kuzucuoglu et al., 1998
5.	8,2	Acıgöl	sediment cores in the late Pleistocene Eski Acıgöl maar, Tephra layer T13 (radiocarbon)	Kuzucuoglu et al., 1998
6.	7,2±0,9	Erciyes	lava-flow (Karagüllü) (cosmogenic ^{36}Cl)	Sarıkaya et al., 2017
7.	7,7±0,4	Erciyes	lava-flow (Perikartın) (cosmogenic ^{36}Cl)	Sarıkaya et al., 2017
8.	8,8±0,6	Erciyes	lava-flow (Dikkartın) (cosmogenic ^{36}Cl)	Sarıkaya et al., 2017
9.	8,9±0,6	Hasandağ	pumices collected from the summit of Big Hasandağ (U-Th/He method measured on zircon crystals)	Schmitt et al., 2014
10.	9,5±0,2	Erciyes	ash-flow (Erciyes) (^{14}C)	Sarıkaya et al., 2006
11.	9,8	Acıgöl	sediment cores in the late Pleistocene Eski Acıgöl maar, Tephra layer T10 (radiocarbon)	Kuzucuoglu et al., 1998
12.	13±5	Erciyes	cinder cone basalt (K-Ar)	Doğan-Külahcı, 2015
13.	14	Acıgöl	sediment cores in the late Pleistocene Eski Acıgöl maar, Tephra layer (radiocarbon)	Kuzucuoglu et al., 1998
14.	16	Acıgöl	Acıgöl maar (U-Th)	Roberts et al., 2001
15.	19	Acıgöl	acidic tephric layer with sphene and zircon (radiocarbon)	Kuzucuoglu et al., 1998
16.	20±6	Acıgöl	Guneydag dome (fission track age)	Bigazzi et al., 1993
17.	20,3±0,6	Acıgöl	Acıgöl maar, obsidian clast nearly aphyric (U-Th/He)	Schmitt et al., 2011
18.	22,3±1,1	Acıgöl	Karnıyarık, rhyolitic lava nearly aphyric (U-Th/He)	Schmitt et al., 2011
19.	23,2±3	Acıgöl	Kaleci, rhyolitic lava nearly aphyric (U-Th/He)	Schmitt et al., 2011
20.	23,8±0,9	Acıgöl	Güneydağ, rhyolitic lava nearly aphyric (U-Th/He)	Schmitt et al., 2011
21.	24,9±0,9	Acıgöl	Korudağ, rhyolitic lava nearly aphyric (U-Th/He)	Schmitt et al., 2011
22.	25±8	Erciyes	cinder cone lava-flow (Avşar Vilage) (K-Ar)	Doğan-Külahcı, 2015
23.	25,9±0,6	Acıgöl	Tepeköy, rhyolitic lava nearly aphyric (U-Th/He)	Schmitt et al., 2011
24.	26±1,5	Acıgöl	Kuzey, rhyolitic lava nearly aphyric (U-Th/He)	Schmitt et al., 2011
25.	28,9±1,5	Hasandağ	pumices collected from the flank of the volcano (U-Th/He method measured on zircon crystals)	Schmitt et al., 2014
26.	29±1	Hasandağ	from the summit (K-Ar)	Kuzucuoglu et al., 1998
27.	32±3	Acıgöl	south of Kocadağ (K-Ar)	Türkecan et al., 2004
28.	33±2	Hasandağ	from the summit (K-Ar)	Kuzucuoglu et al., 1998
29.	36,1±1,1	Erciyes	lava-flow (Çarık) (cosmogenic ^{36}Cl)	Sarıkaya et al., 2017
30.	40±7	Erciyes	fissure basalt (Karagüllü) (K-Ar)	Doğan-Külahcı, 2015
31.	45±5	Erciyes	basaltic lava (Sürtme Plateau) (K-Ar)	Doğan-Külahcı, 2015
32.	75	Acıgöl	Taşkesik, lava dome	Bigazzi et al., 1993
33.	80±10	Erciyes	augite-hypersthene andesite, lava-flow (Karigtepe) (K-Ar)	Notsu et al., 1995

34.	93±11	Erciyes	cinder cone lava-flow (north of Develi) (K-Ar)	Doğan-Külahcı, 2015
35.	93±2	Acıgöl	Boğazköy (obsidian)	Türkecan et al., 2004
36.	96,0±13,0	Acıgöl	basaltic lava (Karnıyarık Hill) (Ar-Ar)	Doğan, 2011
37.	98,4±3,6	Erciyes	lava-flow (Çarık) (kosmogenic ^{36}Cl)	Sarıkaya et al., 2017
38.	102±7	Erciyes	cinder cone basalt (south of Erciyes) (K-Ar)	Doğan-Külahcı, 2015
39.	110±40	Acıgöl	upper Acıgöl tuff (ITPFT isothermal plateau fission track age)	Druitt et al., 1995
40.	115±7	Erciyes	basaltic lava (Şeyhşaban) (K-Ar)	Doğan-Külahcı, 2015
41.	115±20	Erciyes	dacite-flow (Dikkartın) (Ar-Ar)	Ercan et al., 1994
42.	117±4	Acıgöl	Alacasar, rhyolitic pumice aphyric (U-Th/He)	Schmitt et al., 2011
43.	147±8	Acıgöl	Taşkesik, rhyolitic lava nearly aphyric (U-Th/He)	Schmitt et al., 2011
44.	163±7	Acıgöl	upper Acıgöl tuffs Boğazköy, rhyolitic pumice aphyric (U-Th/He)	Schmitt et al., 2011
45.	170±10	Erciyes	hypersthene andesite, lava-flow (south of Kayseri) (K-Ar)	Notsu et al., 1995
46.	180	Acıgöl	lower Acıgöl tuffs (ITPFT isothermal plateau fission track)	Druitt et al., 1995
47.	190±9	Acıgöl	Boğazköy, rhyolitic lava nearly aphyric (U-Th/He)	Schmitt et al., 2011
48.	190±11	Acıgöl	Kocadağ, rhyolitic lava weakly porphyritic (U-Th/He)	Schmitt et al., 2011

Table S2. General features of the sampling veins.

site	location	sample	band width (cm)	cordinates		strike/dip
SARIHIDIR	1	01	6	0667945E	4290662N	N50E/90
		02	2			
		03	4			
		04	4			
		05	3			
	2	06-1	3	0667666E	4290473N	N85W/90
		06-2	3			
		06-3	3			
BALKAYA	3	11A	1	0658004E	4290500N	N70E/78SE
		11B	0,5			
		12C	0,5			
		12D	1			
	4	A-1	5	0657826E	4290507N	N70W/90
		A-2	5			
		B	3			
		C-1	4			
		C-2	5			
		D-1	5			
		D-2	5			
		E-1	2			
		E-2	3			
		F	4			
		G-1	3			
		G-2	3			
		G-3	3			
		H-1	3			
		H-2	3			
		H-3	3			
		H-4	3			
		H-5	3			
		H-6	3			
		H-7	2			
		I-1	3			
		I-2	3			
		J-1	2			
		J-2	2			

Table S3. Mineralogical and petrographical properties of representative Balkaya and Sarıhıdır travertine samples.

site	group	sample	texture	mineralogy	mineral shape	crystal form	porosity type
BALKAYA	I	A-2	Banded, flow	Mainly calcite	Idiomorph	Needle-shaped	Burrowing
		C					
		E-1					
		F					
		H-6					
	II	A-1	Granular (Mosaic)	Mainly calcite	Xenomorph	Granular	Fenestral
		H-2					
		H-3					
		H-4					
		H-7					
		J-1					
	III	H-5	Granular, flow	Mainly calcite	Xenomorph		Shelter
	IV	G-3	Fine crystalline granular	Mainly calcite	Xenomorph	Granular	Shelter, Fenestral
		11B		Mainly calcite, quartz			
		B		Mainly calcite	Idiomorph	Needle-shaped	Fenestral
SARIHIDIR	I	01	Granular rarely banded (flow)	Mainly calcite, quartz, pyroxene, plagioclase, clay minerals	Idiomorph and xenomorph	Needle-shaped	Shelter
		06-3		Mainly calcite, quartz, epidote, clay, plagioclase		Needle-shaped, granular	
	II	03	Granular (Mosaic)	Mainly calcite, quartz, opaque mineral, feldspar	Xenomorph	Granular	Shelter
		05		Mainly calcite			
	III	02	Banded, flow	Mainly calcite, clay minerals	Idiomorph	Needle-shaped	Shelter
		06-1		Mainly calcite			Shelter
		06-2		Mainly calcite, quartz			Shelter, fenestral
		04		Mainly calcite			Fenestral

Table S4. Summary of MC-ICP-MS Uranium (U)-series age data.

site	location	sample	U (ppm)	±2s	^{232}Th (ppb)	±2s	(^{230}Th/^{232}Th)	±2s	(^{230}Th/^{238}U)	±2s	(^{234}U/^{238}U)	±2s	uncorr. age (ka)	±2s	corr. age (ka)	±2s
SARIHIDIR	**1**	**01**	0,02939	0,00005	71,19	0,21	0,996	0,005	0,7951	0,0038	1,2260	0,0026	109,0	1,0	29	50
		02	0,01044	0,00005	4,798	0,020	1,392	0,033	0,2109	0,0050	1,2833	0,0064	19,45	0,51	8,4	5,7
		03	0,01424	0,00004	7,725	0,026	1,517	0,021	0,2712	0,0038	1,4021	0,0034	23,20	0,36	11,3	6,0
		04	0,00843	0,00004	2,778	0,009	1,705	0,027	0,1851	0,0030	1,3189	0,0053	16,39	0,29	8,8	3,8
		05	0,03015	0,00005	23,334	0,060	1,120	0,010	0,2856	0,0025	1,3396	0,0027	25,88	0,26	7,5	9,8
	2	**06-1**	0,01079	0,00004	31,73	0,10	1,055	0,007	1,0219	0,0077	1,1987	0,0048	188,1	4,2	82	121
		06-2	0,00681	0,00005	16,043	0,069	1,187	0,010	0,9217	0,0093	1,2378	0,0071	138,9	3,2	66	39
		06-3	0,00721	0,00003	9,673	0,022	1,840	0,016	0,8138	0,0077	1,2012	0,0050	117,9	2,2	81	16
BALKAYA	**3**	**11A**	0,016727	0,000007	18,09	0,014	2,221	0,011	0,7917	0,0038	1,5649	0,0030	73,2	0,5	52,1	8,4
		11B	0,016056	0,000005	16,75	0,028	2,462	0,013	0,8464	0,0042	1,5262	0,0029	83,4	0,6	62,8	8,4
		12C	0,013963	0,000003	15,29	0,013	1,710	0,012	0,6171	0,0044	1,4857	0,0019	56,7	0,5	33	10
		12D	0,014266	0,000005	18,82	0,025	2,178	0,012	0,9473	0,0052	1,5161	0,0030	99,6	0,9	73	13
	4	**A-1**	0,025181	0,000009	13,89	0,014	3,660	0,020	0,6651	0,0036	1,2473	0,0021	80,6	0,7	67,3	5,6
		A-2	0,03204	0,00005	7,721	0,013	2,571	0,022	0,2042	0,0018	1,1506	0,0024	21,21	0,21	14,9	3,2
		B	0,017004	0,000013	2,81	0,003	4,696	0,037	0,2561	0,0020	1,1782	0,0021	26,6	0,2	22,4	2,1
		C-1	0,012462	0,000004	5,38	0,004	5,787	0,052	0,8232	0,0073	1,3040	0,0025	103,4	1,5	93,8	3,9
		C-2	0,03360	0,00005	9,583	0,020	7,239	0,053	0,6805	0,0049	1,2825	0,0031	79,70	0,87	73,2	2,6
		D-1	0,02988	0,00006	11,661	0,025	8,103	0,049	1,0423	0,0062	1,3857	0,0030	137,8	1,6	130,1	4,9
		D-2	0,008405	0,000005	3,06	0,004	7,287	0,046	0,8750	0,0054	1,3453	0,0032	107,9	1,2	100,3	3,2
		E-1	0,018412	0,000005	5,60	0,006	9,468	0,041	0,9485	0,0040	1,3368	0,0022	125,1	1,0	118,8	2,9
		E-2	0,018412	0,000004	3,78	0,004	15,083	0,084	1,0193	0,0056	1,3631	0,0022	137,0	1,5	132,9	2,7
		F	0,037433	0,000010	12,56	0,012	9,199	0,034	1,0175	0,0036	1,3489	0,0022	139,6	1,0	132,8	3,9
		G-1	0,008494	0,000003	2,39	0,002	11,037	0,061	1,0238	0,0056	1,3616	0,0028	138,4	1,5	132,8	3,5
		G-2	0,01292	0,00004	0,900	0,002	45,52	0,32	1,0451	0,0078	1,4143	0,0042	132,8	2,0	131,5	2,1
		G-3	0,021214	0,000007	0,2534	0,0003	242,3	1,3	0,9539	0,0049	1,3578	0,0020	122,6	1,1	122,3	1,1
		H-1	0,01237	0,00004	5,726	0,016	7,088	0,057	1,0817	0,0088	1,3436	0,0038	158,7	2,9	149,3	7,5
		H-2	0,00747	0,00003	1,707	0,005	13,49	0,11	1,0152	0,0090	1,3520	0,0043	138,1	2,5	133,6	3,5
		H-3	0,011022	0,000004	3,75	0,003	10,088	0,055	1,1319	0,0062	1,3901	0,0026	161,0	1,9	154,6	6,0
		H-4	0,02601	0,00006	8,926	0,022	9,966	0,048	1,1272	0,0054	1,4032	0,0030	156,1	1,7	149,6	5,8
		H-5	0,006597	0,000002	4,81	0,004	4,179	0,027	1,0052	0,0065	1,3541	0,0025	135,3	1,7	119,9	8,7
		H-6	0,02863	0,00005	19,761	0,059	5,321	0,042	1,2105	0,0091	1,3980	0,0033	183,8	3,4	171	18
		H-7	0,009489	0,000004	9,53	0,009	3,550	0,018	1,1754	0,0059	1,3611	0,0030	184,5	2,4	164	27
		I-1	0,019892	0,000008	12,15	0,012	5,915	0,028	1,1912	0,0055	1,3926	0,0028	179,1	2,1	167	15
		I-2	0,02425	0,00006	15,036	0,045	5,314	0,033	1,0861	0,0064	1,3526	0,0043	157,5	2,2	145	10
		J-1	0,015761	0,000005	19,36	0,024	1,878	0,008	0,7606	0,0032	1,2101	0,0025	104,0	0,8	71	15
		J-2	0,01572	0,00005	12,779	0,041	4,091	0,026	1,0961	0,0069	1,3456	0,0043	162,5	2,5	146	15

Table S5. Rare earth element and Ytriyum (Y) concentrations of the studied carbonate veins (ppb).

site	location	sample	La	Ce	Pr	Nd	Sm	Eu	Tb	Gd	Dy	Ho	Y	Er	Tm	Yb	Lu
SARIHIDIR	1	01	194	351	41	157	34	9	4	28	32	7	218	18	3	20	3
		03	41	93	9	42	8	3	1	10	11	2	80	7	1	8	1
		05	55	104	11	39	8	4	0	5	4	1	45	3	1	3	1
	2	06-1	105	187	23	88	19	13	4	24	36	9	345	38	7	54	9
		06-2	34	71	7	31	12	6	8	35	91	30	1395	134	29	226	37
		06-3	16	32	3	15	3	5	0	4	5	2	69	8	1	11	2
BALKAYA	4	A-2	26	48	9	54	22	18	11	51	110	34	1672	136	25	178	30
		C-2	220	424	81	467	197	73	98	478	935	282	13351	1061	190	1390	228
		D-1	292	558	110	616	259	92	122	608	1161	344	14290	1302	227	1670	268
		G-2	20	32	8	47	26	15	12	61	120	36	1824	145	25	188	32
		H-1	93	161	33	187	74	35	37	190	358	112	5595	437	81	568	97
		H-2	57	100	21	123	53	26	28	136	257	81	3999	308	56	410	66
		H-4	263	497	98	556	234	85	114	555	1060	318	13573	1213	213	1570	250
		H-6	330	628	124	684	284	101	132	651	1250	364	15263	1396	244	1776	282
		I-2	140	292	58	338	149	54	64	323	608	179	8087	655	117	837	134
		J-2	146	281	55	311	131	50	60	288	558	168	7805	636	111	811	136

Table S6. Stable (O and C) isotope data of the carbonate samples (‰). $\delta^{18}O_W$ (fluid) computed for 29°C and 44°C.

site	location	sample	$\delta^{13}C$ (VPDB)	$\delta^{18}O$ (VPDB)	$\delta^{18}O$ (VSMOW)	$\delta^{18}O_W$ (29 ºC) (VSMOW)	$\delta^{18}O_W$ (44 ºC) (VSMOW)
SARIHIDIR	1	01	10,7	-12,0	18,5	-11,7	-8,5
		02	8,9	-16,0	14,5	-15,8	-12,6
		03	8,7	-15,0	15,5	-14,7	-11,6
		04	8,7	-16,2	14,3	-16,0	-12,9
		05	11,1	-12,1	18,4	-11,8	-8,6
	2	06-1	9,3	-13,4	17,1	-13,1	-10,0
		06-2	10,9	-11,6	18,9	-11,2	-8,1
		06-3	9,5	-13,2	17,3	-12,9	-9,8
BALKAYA	3	11A	12,2	-9,8	20,7	-9,4	-6,3
		11B	12,1	-9,5	21,0	-9,1	-5,9
		12C	12,2	-10,1	20,4	-9,7	-6,6
		12D	12,1	-10,0	20,5	-9,6	-6,5
	4	A-1	13,2	-9,7	20,8	-9,3	-6,2
		A-2	12,8	-9,8	20,7	-9,4	-6,3
		B	12,7	-9,9	20,6	-9,5	-6,4
		C-1	13,2	-9,6	20,9	-9,2	-6,0
		C-2	13,2	-9,7	20,8	-9,3	-6,2
		D-1	12,9	-9,6	20,9	-9,2	-6,0
		D-2	12,9	-10,1	20,4	-9,7	-6,6
		E--1	12,6	-10,8	19,7	-10,4	-7,3
		E--2	12,7	-10,7	19,8	-10,3	-7,2
		F	11,8	-11,2	19,3	-10,8	-7,7
		G-1	12,6	-11,3	19,2	-10,9	-7,8
		G-2	12,4	-11,2	19,3	-10,8	-7,7
		G-3	11,5	-11,6	18,9	-11,2	-8,1
		H-1	13,0	-10,2	20,3	-9,8	-6,7
		H-2	13,0	-10,3	20,2	-9,9	-6,8
		H-3	13,0	-10,1	20,4	-9,7	-6,6
		H-4	13,1	-10,4	20,1	-10,0	-6,9
		H-5	13,0	-10,5	20,0	-10,1	-7,0
		H-6	12,9	-10,7	19,8	-10,3	-7,2
		H-7	13,0	-10,6	19,9	-10,2	-7,1
		I-1	13,1	-10,1	20,4	-9,7	-6,6
		I-2	13,0	-9,7	20,8	-9,3	-6,2
		J-1	12,9	-10,0	20,5	-9,6	-6,5
		J-2	12,7	-10,1	20,4	-9,7	-6,6